9-20-2012

Self-Consistent Model Of The Interstellar Pickup Protons, Alfvenic Turbulence, And Core Solar Wind In The Outer Heliosphere

Konstantin V. Gamayunov

Ming Zhang

Hamid K. Rassoul

Nikolai V. Pogorelov

Jacob Heerikhuisen

The Astrophysical Journal, 757:74 (15pp), 2012 September 20 doi:10.1088/0004-637X/757/1/74

SELF-CONSISTENT MODEL OF THE INTERSTELLAR PICKUP PROTONS, ALFVÉNIC TURBULENCE, AND CORE SOLAR WIND IN THE OUTER HELIOSPHERE

Konstantin V. Gamayunov[1], Ming Zhang[1], Nikolai V. Pogorelov[2], Jacob Heerikhuisen[2], and Hamid K. Rassoul[1]
[1] Department of Physics and Space Sciences, Florida Institute of Technology, Melbourne, FL 32901, USA; kgamayunov@fit.edu
[2] Department of Physics and Center for Space Physics and Aeronomic Research, University of Alabama, Huntsville, AL 35899, USA
Received 2012 May 2; accepted 2012 July 31; published 2012 September 5

ABSTRACT

A self-consistent model of the interstellar pickup protons, the slab component of the Alfvénic turbulence, and core solar wind (SW) protons is presented for $r \geqslant 1$ along with the initial results of and comparison with the *Voyager 2* (*V2*) observations. Two kinetic equations are used for the pickup proton distribution and Alfvénic power spectral density, and a third equation governs SW temperature including source due to the Alfvén wave energy dissipation. A fraction of the pickup proton free energy, f_D, which is actually released in the waveform during isotropization, is taken from the quasi-linear consideration without preexisting turbulence, whereas we use observations to specify the strength of the large-scale driving, $C_{\rm sh}$, for turbulence. The main conclusions of our study can be summarized as follows. (1) For $C_{\rm sh} \approx 1$–1.5 and $f_D \approx 0.7$–1, the model slab component agrees well with the *V2* observations of the total transverse magnetic fluctuations starting from ∼8 AU. This indicates that the slab component at low-latitudes makes up a majority of the transverse magnetic fluctuations beyond 8–10 AU. (2) The model core SW temperature agrees well with the *V2* observations for $r \gtrsim 20$ AU if $f_D \approx 0.7$–1. (3) A combined effect of the Wentzel–Kramers–Brillouin attenuation, large-scale driving, and pickup proton generated waves results in the energy sink in the region $r \lesssim 10$ AU, while wave energy is pumped in the turbulence beyond 10 AU. Without energy pumping, the nonlinear energy cascade is suppressed for $r \lesssim 10$ AU, supplying only a small energy fraction into the *k*-region of dissipation by the core SW protons. A similar situation takes place for the two-dimensional turbulence. (4) The energy source due to the resonant Alfvén wave damping by the core SW protons is small at heliocentric distances $r \lesssim 10$ AU for both the slab and the two-dimensional turbulent components. As a result, adiabatic cooling mostly controls the model SW temperature in this region, and the model temperature disagrees with the *V2* observations in the region $r \lesssim 20$ AU.

Key words: interplanetary medium – solar wind – Sun: heliosphere – turbulence – waves

Online-only material: color figures

1. INTRODUCTION

As the Sun moves through the local interstellar medium (LISM), neutral atoms of the LISM constantly enter the heliosphere due to the relative motion of the Sun with respect to the interstellar medium. These neutrals (mostly H) may be ionized inside of the heliosphere due to the charge exchange with the solar wind (SW) ions (mostly H^+) and/or by the solar ultraviolet radiation producing the so-called interstellar pickup ions (PUIs). The speed of the original interstellar neutrals is very small with respect to the Sun, being about 21–26 km s^{-1} (McComas et al. 2012). As a result, at the instant of the PUI production, their velocity in the frame comoving with the SW flow is close to the local SW velocity but directed toward the Sun. A component of the PUI velocity perpendicular to the interplanetary magnetic field (IMF) causes the Lorentz force to gyrate ions about the IMF. As a result, PUIs get picked up by the SW flow in the direction perpendicular to the IMF on a timescale of the proton gyroperiod (∼10 s at the Earth orbit). An ion pickup in the direction parallel to the IMF is a more complicated process, and it takes place on a larger timescale compared to the pickup perpendicular to the IMF. Therefore, the newly born PUIs obtain the ring-beam phase space distribution function (PSDF) almost instantly after their production. This ring-beam distribution, however, is unstable with respect to the Alfvén and fast magnetosonic wave generation (e.g., Wu & Davidson 1972; Gary & Madland 1988). The wave generation during instability causes diffusion of the initial ring-beam distribution in the velocity phase space on a timescale of about a hundred of the proton gyroperiods (Florinski et al. 2010). The preexisting background waves in the SW are also able to resonate with the newly born PUIs providing an additional energization and/or pitch-angle scattering. In the super-Alfvénic SW, the above wave–ion interaction mainly causes a pitch-angle diffusion resulting in the nearly isotropic bispherical PSDF (e.g., Galeev & Sagdeev 1988; Huddleston & Jonstone 1992). In the frame comoving with the SW flow, the bulk velocity of the bispherical distribution is parallel to the IMF, being about Alfvén speed. Thus, the PUI parallel velocity with respect to the Sun approaches the SW velocity parallel to the IMF, and the above pitch-angle diffusion completes the proton pickup after a typical scattering time of hundred of the proton gyroperiods.

After they are picked up, the PUIs convect with the SW, while experiencing adiabatic cooling in the expanding SW flow along with a stochastic acceleration due to the SW turbulence (e.g., Isenberg 2005). At the heliospheric termination shock (TS), the PUIs may participate in the diffusive shock acceleration process producing the so-called TS particles (Stone et al. 2005), and/or the anomalous component of cosmic rays (e.g., le Roux & Webb 2009). So the PUI distribution function developed before the TS forms a seed population for the shock acceleration and is one of the crucial elements in the TS acceleration process. From the global heliospheric perspective, a continuous pickup process slows down the SW, while PUIs produced start to increasingly dominate the total kinetic pressure for $r \gtrsim 10$ AU (e.g., Isenberg 1986; Burlaga et al. 1994). The PUI kinetic pressure dominates

both the SW ram pressure and the IMF pressure downstream of the TS where the PUIs are a dominant player. A modification of the large-scale SW properties due to the PUIs may influence the strength, position, and internal structure of the heliospheric TS (e.g., Kucharek & Scholer 1995; Zank et al. 1996; Isenberg 1997). The pickup protons constitute a majority of the PUIs in the SW, and in the present study we consider the pickup protons only. To model their global evolution, we use a kinetic equation that includes spatial transport with the SW velocity, adiabatic cooling/heating due to the divergence/convergence of the SW flow, the proton energy diffusion due to the second-order Fermi mechanism, and a source of the pickup protons due to the charge exchange between the interstellar H and the core SW protons (e.g., Isenberg 2005).

Alfvén and fast magnetosonic waves generated during isotropization of the newly born PUIs represent a local source of wave energy in the region $r \gtrsim 10$ AU, where an effect of PUIs becomes important. The locally generated waves feed the background SW turbulence, participating in the nonlinear energy cascading to the smaller spatial scales, heating the PUIs themselves, and ultimately heating the core SW particles due to the resonant damping at small scales. An understanding of the turbulence generation, transport, and evolution in the global heliosphere is important for both heliospheric physics and space weather applications. For example, SW turbulence plays a key role in the scattering of solar energetic particles (e.g., Bieber et al. 1994), in the cosmic ray scattering and transport (e.g., Florinski et al. 2003), and in the modulation of galactic cosmic rays (e.g., Zank et al. 1998). The solar energetic particles and galactic cosmic rays pose major radiation hazards for space hardware, astronauts, polar flights, and communication/navigation systems. One of the approaches to treating the turbulence evolution in SW is a phenomenological approach that describes the evolution of energy-containing eddies without specifying details of the nonlinear wave–wave interaction that produces the turbulent cascade (e.g., Matthaeus et al. 1994, 1996; Zank et al. 1996, 1998, 2012; Smith et al. 2001, 2006; Isenberg et al. 2003, 2010; Isenberg 2005; Breech et al. 2005, 2008; Oughton et al. 2011). This approach gives the radial evolution of the turbulent energy, cross helicity, and correlation length in a steady, radially expanding SW. Observations of the IMF fluctuations at 1 AU show that fluctuation energy at magnetohydrodynamic (MHD) scales is made up of about 80% of the two-dimensional component (the wave vector is quasi-perpendicular to the mean magnetic field), and about 20% of the slab component (the wave vector is parallel/antiparallel to the mean magnetic field; e.g., Bieber et al. 1996). This partitioning between the two-dimensional and slab fluctuations is most appropriate for the slow SW as shown by Dasso et al. (2005). These two turbulent components demonstrate a quite different radial evolution. For example, the PUI generated waves have relatively high frequencies and wave energy is injected into the slab component only, while the SW stream shear and/or compression drive both turbulent components, but in the region of much lower frequency. These differences encouraged Oughton et al. (2011) to extend the outlined phenomenological approach, and to develop a two-component model that treats fluctuations as an admixture of two incompressible components: a quasi-two-dimensional turbulence and a slab-wave-like turbulence.

Smith (2003) analyzed the turbulent magnetic fluctuations at large distances and different heliolatitudes using *Ulysses* data. The low-latitude results from the papers by Smith (2003) and Bieber et al. (1996) can be interpreted as indicating that the larger distances are associated with increasing energy in the slab component. For example, the slab fraction was often $\gtrsim$50% in 1992 when *Ulysses* was at about 5 AU and low latitudes. This observational trend is similar to the model results presented by Oughton et al. (2011), where they showed that the wave-like Alfvénic turbulence starts to grow from about 3–4 AU, and it dominates the two-dimensional component at the heliocentric distances beyond ~10 AU. Our own independent results, which will be presented in this study, also show that the total transverse magnetic fluctuations extracted from the *Voyager 2* (*V2*) data agree very well with the model slab component starting from about 8–10 AU (see Figure 7(c) below). So the observational and model results suggest that the slab component probably dominates the two-dimensional turbulence at low latitudes starting from about 8–10 AU. For this reason, we model the slab component only in this initial study. In contrast to the above phenomenological approach, we employ a more detailed approach to describe the wave-like Alfvénic turbulence in the heliocentric region $r \geqslant 1$ AU. Namely, we use a kinetic equation for the Alfvén wave power spectral density (PSD). This equation includes the wave PSD transport in the expanding SW, explicit wave damping due to the resonant ion cyclotron interaction with the core SW protons, the wave PSD source due to isotropization of the newly born interstellar pickup protons, the driving effect of the SW flow shear/compression, and, in addition to a pure quasi-linear approximation, the wave energy diffusion in wave number space due to the nonlinear wave–wave interaction.

The nonlinear wave–wave interaction causes the wave energy to cascade to larger wave numbers, ultimately leading to the wave energy dissipation at small scales and heating of the core SW particles. This closes the PUIs–waves–SW chain. Starting from the work by Williams et al. (1995), it is widely believed that heating of the core SW protons in the outer heliosphere is significantly controlled by turbulent dissipation of the Alfvén and/or fast magnetosonic waves generated during isotropization of the newly born interstellar pickup protons. In short, Williams et al. have taken the wave energy generated during a quasi-linear isotropization of the newly born interstellar pickup protons to be the so-called bispherical value, $\Delta E_{\rm bs} = 0.5 m_p U_{\rm sw} V_A$, where m_p is the proton mass, and $U_{\rm sw}$ and V_A are the SW and Alfvén speed, respectively (Galeev & Sagdeev 1988; Huddleston & Jonstone 1992; Williams & Zank 1994). The bispherical value should be considered as an upper limit for the wave energy released during the PUI isotropization. Then, Williams et al. have assumed that a constant fraction f_D of the bispherical value would actually appear as a heat source in the core SW temperature equation. To fit the model temperature profile to the core SW temperature observed by *V2*, Williams et al. have adopted $f_D = 0.02$ in their work. Why only such a small fraction of $\Delta E_{\rm bs}$ is needed to fit the core SW temperature observations has been an ongoing point of discussion (see Isenberg et al. 2003 and references therein). Two extreme possibilities to decrease f_D have been suggested. First, one may assume that a maximum available free energy of the PUIs is injected in SW during the PUI isotropization, but the other effects such as the second-order Fermi energization of the PUIs, damp a majority of the wave energy before the energy can be transferred into the wave number region where the dissipation by SW takes place (e.g., Williams et al. 1995; Chalov et al. 2006). Second, some physical mechanisms may only allow a small fraction of $\Delta E_{\rm bs}$ to be injected in the SW turbulence during the PUI isotropization (e.g., Isenberg et al. 2003). Of course, a combination of these two extremes can also take place. To the best of our knowledge, there are only

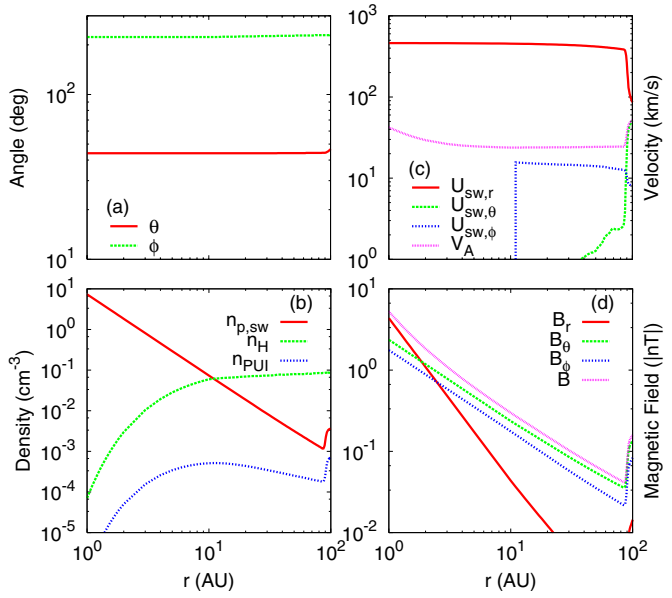

Figure 1. (a) Polar angle θ and azimuthal angle ϕ along the selected SW stream line that goes through the point $(r, \theta, \phi) = (1\,\mathrm{AU}, 44^\circ, 223^\circ)$. (b) Number density of the core SW protons, $n_{p,\mathrm{sw}}$, interstellar hydrogen, n_{H}, and pickup protons, n_{PUI}, along the stream line. (c) Components of the SW velocity and Alfvén speed along the stream line. (d) Absolute values of the IMF components and the total magnetic field along the stream line.

(A color version of this figure is available in the online journal.)

two groups which have tried to provide a rigorous quantitative foundation for the fraction f_D. The original results of these two groups are presented in the papers by Isenberg et al. (2003; they obtained $f_D \approx 0.3$) and by Chalov et al. (2006; they obtained $f_D \approx 0.05$). Currently, the details of the core SW heating in the outer heliosphere are far from being well understood both qualitatively and quantitatively, particularly because a very different value for f_D is used in different studies.

To describe the core SW heating, we finally need to include the core SW evolution in our model. In this study, we consider the core SW protons only, omitting the heavy SW ions and electrons. We assume that SW protons have a Maxwellian distribution in the frame comoving with the bulk SW flow. Then, a three-dimensional distribution of the core SW proton density is taken from the global MHD-plasma/kinetic-neutral model of the heliosphere–LISM interaction (Pogorelov et al. 2008; Heerikhuisen et al. 2008). Note that the MHD/kinetic model actually provides a total density of the core SW protons and PUIs. However, the PUI contribution in the total density is small in the region considered in this study (see Figure 1(b)), and we regard the total density from the MHD/kinetic model as the core SW proton density. With the MHD/kinetic model, we only need a governing equation for the core SW temperature to describe the SW evolution. The temperature equation is well known (e.g., Williams et al. 1995; Isenberg et al. 2003), and it includes adiabatic cooling/heating of the core SW protons along with the energy source due to the Alfvén wave dissipation.

This article is organized as follows. In Section 2, a set of the governing equations is given along with a discussion of the used assumptions and approximations. In the same section, we present the radial profiles of the utilized SW parameters that are taken from the global MHD-plasma/kinetic-neutral model of the heliosphere–LISM interaction. We also specify the boundary conditions for all the governing equations. In Section 3, we present our initial results for the pickup protons, Alfvénic turbulence, and core SW protons in the region $r \geqslant 1$ AU along with discussion and comparison with the *V2* observations. In Section 4, we discuss the contribution of the two-dimensional turbulence in heating of the core SW protons. Finally, in Section 5, we provide a summary and our conclusions.

2. MODEL

2.1. Governing Equations

2.1.1. Kinetic Equation for PUIs

The newly born PUIs have a ring-beam PSDF, which is unstable with respect to the Alfvén and fast magnetosonic wave generation (e.g., Wu & Davidson 1972; Gary & Madland 1988). The instability causes wave generation and diffusion of the initial ring-beam distribution in the velocity phase space. There is mainly a pitch-angle diffusion in the super-Alfvénic SW, and the resulting PSDF is nearly isotropic. In this situation, an anisotropic correction to the isotropic part of the PSDF is small if we are only interested in the PUI evolution on a timescale greater than a typical isotropization time. So, to describe the PUI evolution on a large timescale, we may use the pitch-angle average PSDF, $f(\mathbf{x}, v, t)$, instead of the full distribution function $F(\mathbf{x}, v, \mu, t) = f(\mathbf{x}, v, t) + g(\mathbf{x}, v, \mu, t)$, where v and μ are the PUI speed and pitch-angle cosine, respectively, $f(\mathbf{x}, v, t) = 0.5 \int F(\mathbf{x}, v, \mu, t) d\mu$, $\int g(\mathbf{x}, v, \mu, t) d\mu = 0$, and $|g/f| \ll 1$. The transport equation for $f(\mathbf{x}, v, t)$ can be derived from the well-known gyroaverage quasi-linear kinetic equation for $F(\mathbf{x}, v, \mu, t)$ (e.g., Schlickeiser 1989). In this study, we further simplify the governing equation for PUIs, taking into account that cross helicity of the slab turbulence vanishes beyond ~10 AU (Roberts et al. 1987a, 1987b; Oughton et al. 2011). So the intensities of waves propagating parallel and antiparallel to the IMF are equal, and as a result, all the terms related to the mixed pitch-angle–velocity diffusion disappear from the resulting transport equation (e.g., Schlickeiser 1989). Then, a radial inhomogeneity of the PUI distribution is small beyond 10 AU, and we may omit the spatial diffusion term in the governing equation as well. Finally, the pickup protons constitute a majority of the PUIs in the SW, and in the present study we consider the pickup protons only in keeping the "PUIs" acronym for them.

The resulting kinetic equation for the pitch-angle average distribution function of PUIs takes the following form (e.g., Isenberg 2005; Chalov et al. 2006):

$$\frac{\partial f(\mathbf{x}, v, t)}{\partial t} + \mathbf{U}_{\mathrm{sw}} \frac{\partial f}{\partial \mathbf{x}} - \frac{\nabla \mathbf{U}_{\mathrm{sw}}}{3} v \frac{\partial f}{\partial v} = \frac{1}{v^2} \frac{\partial}{\partial v} \left(v^2 D_{\mathrm{F}} \frac{\partial f}{\partial v} \right) + S_{\mathrm{PUI}}(\mathbf{x}, v, t), \quad (1)$$

where $\mathbf{U}_{\mathrm{sw}}$, D_{F}, and S_{PUI} are the SW velocity, the Fermi diffusion coefficient, and the PUI source due to the charge exchange between the SW protons and interstellar H, respectively. Equation (1) is written in a mixed coordinate frame where the spatial coordinate $\mathbf{x}$ is measured in the solar frame, while PUI velocity $\mathbf{v}$ is measured in the frame comoving with the SW bulk flow. The second term on the left-hand side of Equation (1) describes the PUI transport with the SW velocity, and the third term takes into account adiabatic cooling/heating due to the divergence/convergence of the SW flow. The two terms on the right-hand side describe diffusion in speed due to the interaction with waves propagating in the opposite directions and the PUI production due to the charge exchange, respectively. The

number density of the pickup protons in the phase space element is given by the equation $dn(\mathbf{x}, v, t) = f(\mathbf{x}, v, t)4\pi v^2 dv$.

The Fermi diffusion coefficient has the following form (e.g., Schlickeiser 1989; Isenberg 2005):

$$D_{\rm F}(\mathbf{x}, v, t) = \frac{1}{2}\int_{-1}^{1} d\mu \left(D_{vv} - \frac{D_{\mu v}^2}{D_{\mu\mu}}\right),$$

where D_{vv}, $D_{\mu v}$, and $D_{\mu\mu}$ are the usual quasi-linear diffusion coefficients in the (v, μ)-space (e.g., Galeev & Sagdeev 1988; Schlickeiser 1989). In this initial study, we are focused on the near-ecliptic heliospheric region in the direction of the current *V2* location. The IMF in this region is nearly azimuthal beyond the heliocentric distance ~10 AU where the effect of the PUIs becomes important. This suggests that the newly born PUIs have pitch angles close to 90° in the frame comoving with the SW. It is expected in this case that mainly left-hand polarized waves (i.e., Alfvén waves) propagating parallel and antiparallel to the IMF are generated during the PUI isotropization (e.g., Galeev & Sagdeev 1988; Huddleston & Jonstone 1992). The Alfvénic turbulence locally generated by the PUIs dominates the slab turbulence transported from the Sun at heliocentric distances beyond ~10 AU (Oughton et al. 2011). So, in the framework of linear approximation, we do not have the right-hand polarized fast magnetosonic waves propagating parallel and/or antiparallel to the average magnetic field. Consequently, the PUIs with a particular (v, μ)-pair interact with the counter-propagating Alfvén waves only, and the Fermi diffusion coefficient is zero in this approximation. It is possible, however, that nonlinear processes can produce the fast magnetosonic waves propagating in the direction of the field-aligned PUI propagation that are falling into a resonance with the same PUIs. Then, the second-order Fermi acceleration can operate. However, Isenberg (2005) showed that the effect of the second-order Fermi acceleration is small for PUIs. So we neglect all nonlinear processes and adopt a vanishing diffusion coefficient,

$$D_{\rm F}(\mathbf{x}, v, t) = 0, \tag{2}$$

in this study. Under this approximation, Equation (1) does not depend on the Alfvén wave evolution explicitly. The PUIs and waves only interact during an initial isotropization stage. This initial stage results in the wave generation and a corresponding energy loss by PUIs that should be explicitly included in the PUI production term in Equation (1).

At the instant of PUI production, their speed in the frame comoving with the SW flow is equal to the local SW speed. However, part of the PUI initial energy is spent to generate Alfvén and fast magnetosonic waves during isotropization. Therefore, after a typical isotropization time, an isotropic part of the newly born PUI distribution can be approximated by a sphere in the velocity space with a radius, $V_{\rm sp}$, slightly less than $U_{\rm sw}$. In the super-Alfvénic SW, keeping only the terms of the order of $V_A/U_{\rm sw}$, we get $V_{\rm sp} = U_{\rm sw} - V_A/2$ (e.g., Fahr & Chashei 2002; Chalov et al. 2006). So the PUI source in Equation (1) takes the following form (e.g., Chalov et al. 2006):

$$S_{\rm PUI}(\mathbf{x}, v, t) = \frac{\beta_i n_{\rm H}}{4\pi V_{\rm sp}^2}\delta(v - V_{\rm sp}), \tag{3}$$

where $n_{\rm H}$ and β_i are the density of the interstellar H and their ionization rate, respectively. According to the work of Ruciński et al. (1996), the photoionization rate is at least seven times smaller than the charge-exchange ionization rate at 1 AU. Considering the charge exchange between the core SW protons and interstellar H as the primary source of the PUIs, we can explicitly specify the ionization rate as

$$\beta_i(\mathbf{x}, U_{\rm sw}, t) = \sigma_{\rm ex}(U_{\rm sw})\, U_{\rm sw} n_{p,\rm sw},$$

where $\sigma_{\rm ex}$ is the H–p charge-exchange cross section, and $n_{p,\rm sw}$ is the core SW proton density. The H–p charge-exchange cross section is taken according to the report by Barnett (1990), and $\sigma_{\rm ex} \approx 2 \times 10^{-15}$ cm^2 for the proton energy of about 1 keV.

2.1.2. Kinetic Equation for Alfvénic Turbulence

To describe the evolution of the Alfvén wave PSD, $W(\mathbf{x}, k, t)$, we use the quasi-linear kinetic equation but with the additional nonlinear terms included. Considering only the field-aligned propagating Alfvén waves (see Section 1 for justification), the governing equation takes the following form (Hollweg 1974; Chalov et al. 2006; Jiang et al. 2009; Oughton et al. 2011):

$$\frac{\partial W(\mathbf{x}, k, t)}{\partial t} + (\mathbf{U}_{\rm sw} + \mathbf{v}_{\rm g})\frac{\partial W}{\partial \mathbf{x}} + \frac{3\nabla \mathbf{U}_{\rm sw}}{2} W = 2\gamma_{\rm sw}(\mathbf{x}, k, t)\, W + S_{\rm w}(\mathbf{x}, k, t) + \frac{\partial}{\partial k}\left(D_{\rm kk}\frac{\partial W}{\partial k}\right) + \left(\frac{\delta W}{\delta t}\right)_{\rm LS}. \tag{4}$$

In Equation (4), k is the wave normal number ($k > 0$ for Alfvén waves propagating parallel to the IMF, and $k < 0$ otherwise), $\mathbf{v}_{\rm g}$ is the wave group velocity, $\gamma_{\rm sw}$ is the wave damping rate due to the resonant ion cyclotron interaction with the core SW protons, $S_{\rm w}$ is the source of the Alfvén wave PSD, $D_{\rm kk}$ is the wave number diffusion coefficient due to the nonlinear wave–wave interaction, and the term $(\delta W/\delta t)_{\rm LS}$ takes into account the effects of the large-scale SW flow shear/compression and gradients of the large-scale fields on Alfvénic fluctuations. Similar to Equation (1), Equation (4) is also written in a mixed coordinate frame where spatial coordinates are measured in the solar frame, while all the wave characteristics are measured in the frame comoving with the SW. The PSD is normalized to the total energy density of Alfvén waves propagating parallel and antiparallel to the IMF, i.e., $\int_{-\infty}^{+\infty} W(\mathbf{x}, k, t)dk = B_{\rm w}^2(\mathbf{x}, t)/8\pi$, where $B_{\rm w}^2$ is the squared magnetic field of the Alfvénic fluctuations. The Alfvén wave group velocity is restricted by the Alfvén speed, and it may be safely neglected in the super-Alfvénic SW. Then, in the radially expanding SW, the last two terms in the left-hand side of Equation (4) can be reduced to $U_{\rm sw}/r^3\partial(r^3 W)/\partial r$, where r is the heliocentric distance. This is the well-known Wentzel–Kramers–Brillouin (WKB) result (e.g., Chalov et al. 2006). Thus, the spatial transport of the Alfvén wave PSD inside the TS is nearly identical to that of the WKB theory.

In accordance with Equation (2), the resonant wave damping due to the PUI stochastic acceleration is negligible. As a result, the wave kinetic equation (4) does not include the corresponding damping rate. This is one of the major differences between our model and the model presented by Chalov et al. (2006). The Chalov et al. results show that the second-order Fermi energization of PUIs reabsorbs practically all wave energy generated during the PUI isotropization, leaving only a small energy fraction to heat the core SW protons. Contrary to this, we consider the nonlinear transformation of the PUI generated Alfvén waves into the fast magnetosonic waves to be weak, resulting in $D_{\rm F} \approx 0$. This is supported by analysis of the Alfvén-wave-induced scattering by the cold plasma ions, which shows that the intensity of the oppositely propagating fast magnetosonic waves is low (e.g., Galeev & Sagdeev 1988).

To evaluate the Alfvén wave damping rate due to the resonant ion cyclotron interaction with the core SW protons, we assume that the core SW protons have a Maxwellian PSDF in the frame comoving with the SW bulk flow, i.e.,

$$F_{\rm sw}(\mathbf{x}, v, t) = \frac{n_{p,\rm sw}}{\left(2\pi v_{\rm sw}^2\right)^{3/2}} \exp\left\{-\frac{v^2}{2v_{\rm sw}^2}\right\}, \; v_{\rm sw}^2 = \frac{T_{\rm sw} k_B}{m_p}, \tag{5}$$

where $T_{\rm sw}$ is the temperature of the core SW protons, and $k_{\rm B}$ is the Boltzmann constant. Using distribution (5), we can calculate damping rates for the left-hand polarized Alfvén waves propagating parallel and/or antiparallel to the IMF (e.g., Kennel & Petschek 1966):

$$\gamma_{\rm sw}(\mathbf{x}, k, t) = -\frac{n_{p,\rm sw}}{(n_{p,\rm sw} + n_{\rm PUI})}\sqrt{\frac{\pi}{2}}\frac{\Omega_p(\Omega_p - \omega)^2}{(2\Omega_p - \omega)v_{\rm sw}|k|} \times \exp\left\{-\frac{(\Omega_p - \omega)^2}{2k^2 v_{\rm sw}^2}\right\}, \tag{6}$$

where $n_{\rm PUI}$ is the PUI number density, Ω_p is the proton gyrofrequency, and the wave frequency $\omega = \omega(k)$ in the cold electron–proton plasma has the following form (e.g., Akhiezer et al. 1975):

$$\omega(k) = |k| V_A \left(\sqrt{\frac{k^2 V_A^2}{4\Omega_p^2} + 1} - \frac{|k| V_A}{2\Omega_p}\right). \tag{7}$$

The IMF in the near-ecliptic heliospheric region is nearly azimuthal beyond the heliocentric distance ~10 AU where the effect of the PUIs becomes important. In this region, the newly born PUIs have pitch angles close to 90° in the SW frame, and during isotropization they mainly generate the left-hand polarized Alfvén waves propagating parallel and antiparallel to the IMF. An asymptotic wave PSD calculated in a quasi-linear approximation can be found, for example, in the papers by Galeev & Sagdeev (1988) and Huddleston & Jonstone (1992). This PSD gives us a source term in Equation (4). In the leading order, neglecting small terms of the order of $V_A/U_{\rm sw}$, a source of the Alfvén wave PSD takes the following form (Huddleston & Jonstone 1992):

$$S_{\rm w}(\mathbf{x}, k, t) = f_D \frac{\beta_i n_{\rm H} m_p V_A U_{\rm sw}}{2k_{\rm min}}\left(1 - \frac{k_{\rm min}}{|k|}\right)\frac{k_{\rm min}^2}{k^2},$$
$$k_{\rm min} \leqslant |k| \leqslant k_{\rm max} = \frac{U_{\rm sw}}{V_A} k_{\rm min}, \tag{8}$$

and $S_{\rm w}(\mathbf{x}, k, t) = 0$ for $|k|$ outside of the $[k_{\rm min}, k_{\rm max}]$ region, where $k_{\rm min} = \Omega_p/U_{\rm sw}$, and $f_D = 1$ (see below for more details about f_D). Note that spectral cutoff beyond $k_{\rm max}$ in the Huddleston & Jonstone (1992) formulation is due to the low-frequency approximation ($\omega = |k|V_A$) they used for all k. There is no cutoff if Equation (7) is used instead of the low-frequency limit, while the spectrum in the region $|k| > k_{\rm max}$ is steeper than $\sim k^{-2}$. Below, to keep a conservative estimate for the wave energy injected in the system, we adopt Equation (8).

The total energy density injected per unit time in the waves propagating in both directions is

$$Q_{\rm w}(\mathbf{x}, t) = \int_{-\infty}^{+\infty} S_{\rm w}(\mathbf{x}, k, t)\, dk = f_D \frac{V_A}{U_{\rm sw}}\frac{\beta_i n_{\rm H} m_p U_{\rm sw}^2}{2} = \zeta \frac{\beta_i n_{\rm H} m_p U_{\rm sw}^2}{2}. \tag{9}$$

For $f_D = 1$, this is simply the $V_A/U_{\rm sw}$ fraction of the initial kinetic energy density of PUIs born in a unit of time, which is also a free energy available for the wave generation in the quasi-linear approximation. The same amount of energy (Equation (9)) should be removed from PUIs during their isotropization. This fact is reflected in the PUI source term (3), where $V_{\rm sp}$ is used instead of the initial PUI speed $U_{\rm sw}$. The factor f_D gives us a fraction of the PUI free energy, which is actually released in the waveform during the PUI isotropization. This fraction is related to the fraction of the initial PUI energy ζ, which is sometimes used instead of f_D, as follows $\zeta = f_D V_A/U_{\rm sw}$ (see the right-hand side of Equation (9); e.g., Isenberg et al. 2003). Oughton et al. (2011), for example, used $\zeta = 0.04$ in their calculations that correspond to $f_D \approx 0.5$. The same ζ gives $f_D \approx 0.74$ for the SW parameters from the global MHD-plasma/kinetic-neutral model used in the present study.

It follows from the quasi-linear consideration of the PUI isotropization that $f_D = 1$ if there are no preexisting background waves (e.g., Galeev & Sagdeev 1988; Huddleston & Jonstone 1992). The limit $f_D = 1$, however, should be considered as an upper limit for the wave energy injected in the plasma during the PUI isotropization. For example, the newly born PUIs can potentially diffuse in both directions along the quasi-linear diffusion characteristics that result in the PUI energy increase or decrease. If there are no preexisting background waves that are able to resonate with the PUIs and increase their energy, then the PUI isotropization may only be caused by the PUI generated waves. In this case, the PUIs diffuse in the direction that leads to their energy decrease. This results in $f_D = 1$. In general, however, this situation is unrealistic because, for example, there is a background turbulence transported with the SW. In addition, other sufficiently fast processes not included in Equation (4) might damp some of the wave energy before it is dissipated by the core SW protons. This also leads to an effective decrease of f_D. So in general, f_D should be less than unity. We already mentioned above that Oughton et al. (2011) used $f_D \approx 0.5$ but, for example, Isenberg et al. (2003) adopted a slightly different value of $f_D \approx 0.31$ in their calculations. In principle, a quasi-linear consideration of an initial stage of the PUI isotropization, including the background wave turbulence, will give us a correct f_D for a particular situation. However, this is a very large task, and it should be done separately. In this initial study, we simply use the result from the quasi-linear consideration when there are no preexisting background waves, i.e., $f_D = 1$, except in Figures 7(c) and 10 where we show how the model-*V2* agreement depends on f_D.

The nonlinear wave–wave interaction causes the wave energy transfer in k-space. In this study, we adopt a phenomenological diffusive approximation to treat this nonlinear interaction as a diffusion in k-space (Zhou & Matthaeus 1990). The diffusion coefficient has the following form (Zhou & Matthaeus 1990; Jiang et al. 2009):

$$D_{\rm kk}(\mathbf{x}, k, t) = V_A |k|^{7/2}\sqrt{\frac{W(\mathbf{x}, k, t)}{B^2/4\pi}}\left(1 + \sqrt{\frac{B^2/4\pi}{W(\mathbf{x}, k, t)\, k}}\right)^{-1}, \tag{10}$$

where B is the IMF. Omitting for a moment all the terms in Equation (4), except for the diffusion term, one can see that the diffusion coefficient (Equation (10)) admits the Kolmogorov PSD ($W(k) \sim |k|^{-5/3}$) in the limit of weak magnetic field (the limit of strong turbulence), and the Kraichnan PSD ($W(k) \sim |k|^{-3/2}$) in the opposite case (see the paper by Zhou & Matthaeus

1990 for details). The weak magnetic field approximation has a limited applicability in the outer heliosphere. That is why we use a general formulation for the diffusion coefficient in this study. Note that the diffusion coefficient (Equation (10)) actually takes its Kraichnan limit in the outer heliosphere, except probably at the polar regions.

The last term in the right-hand side of Equation (4) represents the driving effects of the SW flow shear/compression and gradients of the large-scale fields on Alfvénic fluctuations. To approximate these effects, we use results from a widely used phenomenological model of the SW turbulence (see, e.g., Oughton et al. 2011 and references therein),

$$\left(\frac{\delta W}{\delta t}\right)_{\rm LS} = (C_{\rm sh} - \sigma_D \cos^2\Psi) U_{\rm sw} \frac{W(\mathbf{x}, k, t)}{r}, \qquad (11)$$

where Ψ is the Parker spiral angle between the IMF and the radial direction from the Sun. The strength of the shear/compression driving is controlled by the constant $C_{\rm sh}$, and σ_D is the normalized energy difference between the kinetic and magnetic fluctuation components. The product $\sigma_D \cos^2\Psi$ controls the effect of mixing between the large-scale expansion of SW and small-scale Alfvénic fluctuations (e.g., Isenberg et al. 2010), while it is small in the outer heliosphere due to the $\cos^2\Psi$ factor.

To specify the large-scale driving parameters in Equation (11), we use observations. The normalized energy difference is approximately constant with the heliocentric distance (Roberts et al. 1987b). Furthermore, Milano et al. (2004) reported that σ_D at 1 AU almost does not depend on the IMF orientation. So it does not vary strongly with the Parker spiral angle as well. In accordance with the observations reported by Roberts et al. (1987b), below we adopt $\sigma_D = -1/3$. The value of the shear constant was discussed by Breech et al. (2008, Figure 1) in detail. They used *Ulysses* data to construct $C_{\rm sh}$, and in this paper we utilize their results. Because we are going to compare our results with the *V2* data (the heliographic latitude of the current *V2* location is about -30°), the heliographic latitudinal region of interest is 0°–30°, where $1 \leqslant C_{\rm sh} \leqslant 1.5$. Similar to the work of Isenberg et al. 2010, we chose to use $C_{\rm sh} = 1.4$ as the nominal value used throughout this study, while a few results for $C_{\rm sh} = 1$ (e.g., Oughton et al. 2011) are also shown for comparison purposes.

2.1.3. Equation for Core SW Temperature

In this study, we consider the core SW protons only, omitting the other SW ions and electrons. Damping of the Alfvén wave energy due to the resonant ion cyclotron interaction with the core SW protons is, at the same time, the energy source for heating of the core SW protons. This process is currently considered to be a major energy source for SW heating in the outer heliosphere. To describe the wave energy dissipation and SW heating self-consistently, we need a governing equation for the core SW protons as well. We assume in this study that the core SW protons have a Maxwellian distribution in the frame comoving with the SW bulk flow (see Equation (5)). A three-dimensional distribution of the SW proton density is taken from the global MHD-plasma/kinetic-neutral model of the heliosphere–LISM interaction (Pogorelov et al. 2008; Heerikhuisen et al. 2008). Then, to describe the evolution of the core SW temperature, including the effect of the wave source, we use the following equation (e.g., Akhiezer et al. 1975):

$$\frac{\partial T_{\rm sw}(\mathbf{x}, t)}{\partial t} + \mathbf{U}_{\rm sw} \frac{\partial T_{\rm sw}}{\partial \mathbf{x}} + \frac{2\nabla \mathbf{U}_{\rm sw}}{3} T_{\rm sw} = \frac{2}{3 n_{p,\rm sw} k_{\rm B}} S_{\rm T}(\mathbf{x}, t). \qquad (12)$$

The energy source on the right-hand side is due to the Alfvén wave damping, and it has the following form:

$$S_{\rm T}(\mathbf{x}, t) = -2 \int_{-\infty}^{+\infty} \gamma_{\rm sw}(\mathbf{x}, k, t)\, W(\mathbf{x}, k, t)\, dk. \qquad (13)$$

This form explicitly takes into account conservation of energy during the resonant ion cyclotron interaction between waves and the core SW protons.

A set of Equations ((1), (4), and (12)) is used in this study to self-consistently model a system of the PUIs, Alfvénic turbulence, and core SW temperature. However, the global MHD/kinetic model is treated independently, and any feedback of the kinetic processes to the MHD model is neglected at this point.

2.2. SW Parameters

To solve a set of the governing equations, we need to know the global distribution of the SW parameters and interstellar H, namely $\mathbf{U}_{\rm sw}$, V_A, $n_{p,\rm sw}$, $n_{\rm H}$, and $\mathbf{B}$. In this study, we use the SW results from the global MHD-plasma/kinetic-neutral model of the heliosphere–LISM interaction (Pogorelov et al. 2008; Heerikhuisen et al. 2008). This global model is based on a set of MHD equations that describe the SW and PUI evolution. This set is coupled to the Boltzmann kinetic equation that describes the neutral H in the heliosphere and in the LISM. The model treats the ion population as a single fluid whose total pressure is a sum of the electron, thermal ion (SW or LISM), and PUI pressure contributions. The pickup of ions and creation of the new H are included self-consistently through the source integrals in the plasma momentum and energy equations, and in the Boltzmann equation for neutrals.

The MHD/kinetic code uses the Sun centered coordinate system with the x-axis parallel to the Sun's rotation axis, the z-axis lying in the solar ecliptic plane and belonging to the plane defined by the LISM velocity and the x-axis (we neglect a tilt of the Sun's rotation axis with respect to the ecliptic plane), and the y-axis completing a right-handed coordinate system (Pogorelov et al. 2007). Below, we present solutions of the governing equations (1), (4), and (12) only along one SW stream line, namely along the heliocentric direction to the current *V2* location. In the given Cartesian coordinate system, the direction is approximately given by the spherical coordinates $\theta \approx 44^\circ$ and $\phi \approx 223^\circ$, where θ and ϕ are the polar and azimuthal angles in the spherical coordinate system based on the chosen Cartesian system; the θ angle is measured off the z-axis, and the ϕ angle is measured counterclockwise off the x-axis.

Figure 1 shows all the SW parameters along the selected stream line starting from $(r, \theta, \phi) = (1\,\mathrm{AU}, 44^\circ, 223^\circ)$. The TS features appear in Figure 1 at the heliocentric distance $r \approx 86$ AU. The SW flow inside the TS is nearly radial (see Figures 1(a) and (c)) with deceleration due to the production of PUIs. The IMF is almost perpendicular to the radial direction beyond $\sim$10 AU (see Figure 1(d)). The number density of the core SW protons depends on the heliocentric distance as $n_{p,\rm sw} \sim r^{-2}$, and the radial profile of the interstellar H density can be well fitted by the well-known analytical formula (e.g., Fahr 1971; Isenberg et al. 2003; Chalov et al. 2006). For completeness, we also showed in Figure 1(b) the model PUI density along the stream line.

2.3. Boundary Conditions

In this initial study, we present only the stationary solutions of Equations (1), (4), and (12), i.e., $\partial/\partial t = 0$ in all the governing equations. The boundary conditions for the PUI PSDF are $f(r = 1\,\mathrm{AU}, v) = 0$, and $f(\mathbf{x}, v_{\min}) = f(\mathbf{x}, v_{\max}) = 0$, where $v_{\min} = 2\,\mathrm{km\,s^{-1}}$ and $v_{\max} = 10^3\,\mathrm{km\,s^{-1}}$. The boundary condition at $v_{\max}$ is needed where adiabatic cooling takes place, i.e., for $\nabla \mathbf{U}_{\mathrm{sw}} > 0$. This situation takes place inside and outside the TS. The boundary condition at $v_{\min}$ is used in the region of adiabatic heating, i.e., for $\nabla \mathbf{U}_{\mathrm{sw}} < 0$, which takes place in the TS transition region.

To solve Equation (4), we use the following boundary conditions: $\partial W(\mathbf{x}, k_{\min})/\partial k = \partial W(\mathbf{x}, k_{\max})/\partial k = 0$, where $k_{\min} = 0.2\,\mathrm{rad\,AU^{-1}}$ and $k_{\max} = 10^{10}\,\mathrm{rad\,AU^{-1}}$. To specify the Alfvén wave PSD at $r = 1$ AU, we follow the works by Toptygin (1985) and Chalov et al. (2006) with a minor, but quite important, modification. Namely, we took the original PSD from the paper by Chalov et al. (2006, Equation (11)), but filtered this PSD through damping by the core SW protons at $r = 1$ AU. With a high accuracy, the resulting PSD is just the original PSD in the region $[k_{\min}, k_{\mathrm{ext}}]$, where $\partial \gamma_{\mathrm{sw}}(r = 1\,\mathrm{AU}, k_{\mathrm{ext}})/\partial k = 0$, and $W(r = 1\,\mathrm{AU}, k) = 0$ otherwise. So the Alfvén wave PSD at $r = 1$ AU is

$$W(r = 1\,\mathrm{AU}, k) = N \frac{k^2}{\left(k_{\mathrm{cE}}^2 + k^2\right)^{11/6}},$$
$$N = \frac{B_{\mathrm{slab}}^2}{16\pi \int_{k_{\min}}^{k_{\mathrm{ext}}} k^2 \left(k_{\mathrm{cE}}^2 + k^2\right)^{-11/6} dk}, \quad (14)$$

where $k_{\mathrm{cE}} = 2\pi/0.03\,\mathrm{rad\,AU^{-1}}$ (e.g., Isenberg et al. 2003). Then, observations of the SW magnetic field fluctuations at 1 AU show that fluctuation energy is made up of about 80% of the two-dimensional component, and about 20% of the slab component (e.g., Bieber et al. 1996). Adopting this partitioning and using data from the paper of Isenberg et al. (2003), we can estimate $B_{\mathrm{slab}}^2 = 0.9\,\mathrm{nT}^2$.

Finally, the boundary condition for Equation (12) is taken in accordance with the *V2* observations, i.e., $T_{\mathrm{sw}}(r = 1\,\mathrm{AU}) = 7 \times 10^4$ K (e.g., Isenberg et al. 2003).

3. RESULTS

The governing equations used in this study do not include TS related features such as, for example, the diffusive shock acceleration, wave instability in the vicinity of the shock, etc. So in this study, we concentrate on the region inside the TS only.

3.1. PUIs

Figure 2 shows the radial profiles of typical timescales for three terms in Equation (1) along with a typical isotropization timescale for the newly born PUIs. A typical timescale for the radial transport is estimated to be $t_{\mathrm{r}} = r/U_{\mathrm{sw}}$, where U_{sw} is a speed characteristic of the large-scale spatial transport, and r is the heliocentric distance typifying spatial gradient. Similarly, adiabatic cooling/heating timescale is estimated to be $t_{\mathrm{v}} = 3/|\nabla \mathbf{U}_{\mathrm{sw}}|$. The timescale for PUI production is estimated as $t_{\mathrm{PUI}} = (4\pi \int S_{\mathrm{PUI}}(\mathbf{x}, v) v^2 dv/n_{\mathrm{PUI}})^{-1}$. The typical isotropization timescale for the newly born PUIs is taken to be the typical pitch-angle scattering time evaluated at $k_{\mathrm{w}} = 1.5 k_{\min}$, where $\partial S_{\mathrm{w}}(k_{\mathrm{w}})/\partial k = 0$, giving $t_\mu = (\Omega_p 8\pi W(\mathbf{x}, k_{\mathrm{w}}) k_{\mathrm{w}}/B^2)^{-1}$ (e.g., Kennel & Petschek 1966; Joyce et al. 2010). It follows

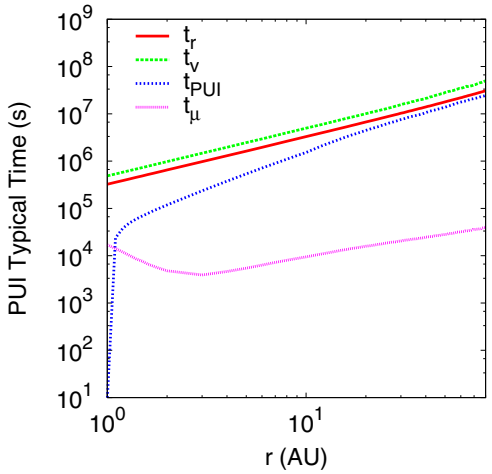

Figure 2. Radial profiles of the typical timescales for three terms in Equation (1) and the typical isotropization timescale for the newly born PUIs. t_{r} is the timescale for spatial transport, t_{v} is the scale for adiabatic cooling, t_{PUI} is the scale for the PUI production, and t_μ is the typical isotropization timescale.
(A color version of this figure is available in the online journal.)

from Figure 2 that the isotropization timescale inside the TS is much smaller than all the timescales in Equation (1). This justifies our approach in describing the PUIs using the pitch-angle average PSDF. In Equation (1) itself, the PUI production is the fastest process inside the TS, while the PUI adiabatic cooling is the slowest one. However, all the timescales are close enough for the heliocentric distances greater than ∼10 AU, where Equation (1) can be characterized by a single timescale of about 10^7 s ≈ 116 days.

The PSDF for PUIs along with the core SW proton distribution are shown in Figure 3. Figure 3(a) shows the PUI distributions for the different heliocentric locations along the selected SW stream line, and the core SW proton distributions are added in Figure 3(b). It follows from Figure 3(a) that the PUIs experience adiabatic cooling inside the TS. A decrease in the PUI speed with the radial distance can be approximated by $v \approx v_{\mathrm{inj}}(r_{\mathrm{inj}}/r)^{2/3}$, where v_{inj} is the speed of the PUI at the heliocentric distance r_{inj}. For example, the PUIs born at $r = 1$ AU have a speed of about $20\,\mathrm{km\,s^{-1}}$ just upstream of the TS located at $r \approx 86$ AU. A combined "SW+PUI" distribution is shown in Figure 3(b). The PSDF of the core SW proton is given by Equation (5), where the SW temperature is driven by Equation (12). All the combined PSDFs demonstrate two well-separated distributions, while a tendency to gradually adjust to each other with distance is observed in both the core SW proton and the PUI distributions.

The radial profiles of the core SW ram/kinetic pressure, the PUI ram/kinetic pressure, and the IMF pressure are shown in Figure 4. Both the core SW ram pressure, $P_{\mathrm{sw,ram}} = n_{p,\mathrm{sw}} m_p U_{\mathrm{sw}}^2$, and the PUI ram pressure, $P_{\mathrm{PUI,ram}}$, simply mimic the SW and PUI density profiles shown in Figure 1(b). These two pressures strongly dominate the corresponding kinetic pressures, $P_{\mathrm{kin}} = m_p 4\pi \int f(v) v^4 dv/3$, inside the TS. The SW ram pressure, in turn, dominates both the PUI ram pressure and the IMF pressure, $P_{\mathrm{mag}} = B^2/8\pi$, controlling the SW dynamics inside the TS. The total kinetic pressure, $P_{\mathrm{kin,tot}}$, is dominated by the core SW protons below $r \approx 3$ AU, while the PUIs control the total kinetic pressure for $r \gtrsim 10$ AU. Downstream of the TS (not shown), the total kinetic pressure dominates all the other pressures, and the PUIs are a dominant player there.

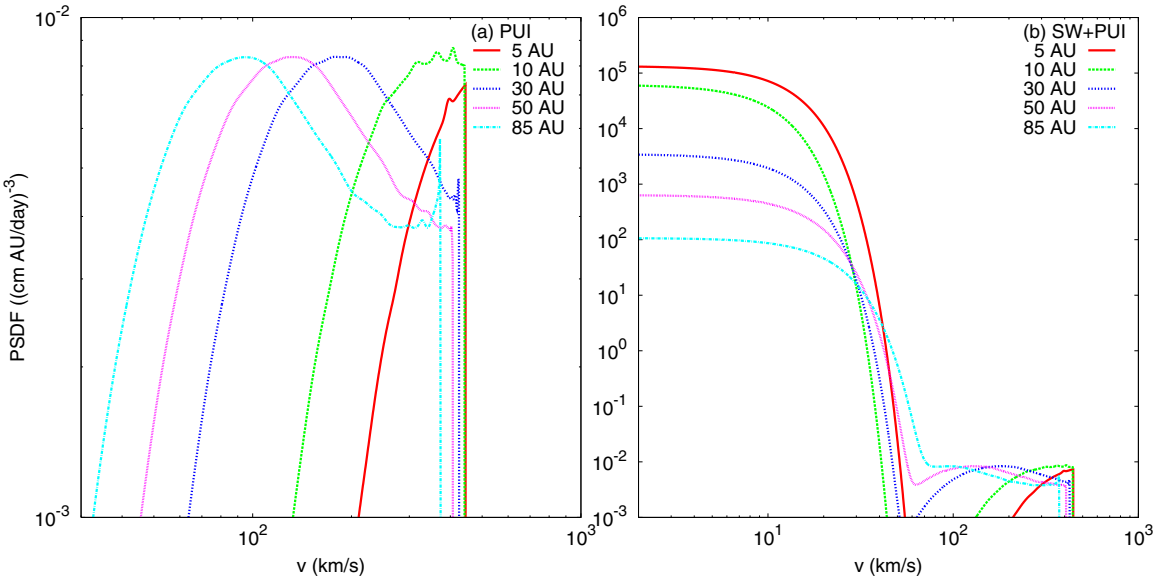

Figure 3. (a) PSDF of PUIs at the different heliocentric locations along the selected SW stream line. (b) Same as (a), except the PSDF of the core SW protons is added. (A color version of this figure is available in the online journal.)

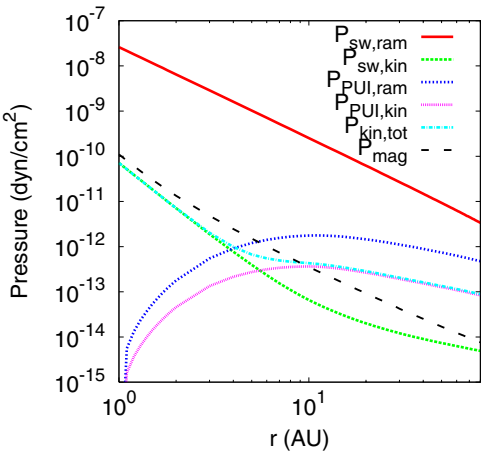

Figure 4. Radial profiles of the core SW ram/kinetic pressure, the PUI ram/kinetic pressure, and the IMF pressure along the selected SW stream line. (A color version of this figure is available in the online journal.)

3.2. Alfvénic Turbulence

Figure 5 shows the source of the wave PSD (8), the wave damping rate (6), and the k-space diffusion coefficient (10) for the different heliocentric locations along the selected SW stream line. It follows from Figures 5(a) and (b) that the maximum of the wave source and the minimum of the wave damping rate are well separated in k-space, while a partial overlap between S_w and $2|\gamma_{sw}|$ still exists. In this case, strictly speaking, the wave damping due to the resonant ion cyclotron interaction with the core SW protons should be included during the PUI isotropization that, in turn, could potentially modify the source term (8). Particularly, the partial overlap between S_w and $2|\gamma_{sw}|$ should disappear. In this initial study, however, we neglect this potential modification. The damping rate in Figure 5(b) strongly dominates the k-space diffusion rate in Figure 5(c). As a result, the diffusion coefficient D_{kk} goes to zero at the wave numbers slightly above the maximum of $|\gamma_{sw}|$.

Figure 6 is similar to Figure 2, except it shows timescales for wave fluctuations derived from Equation (4). Compared to Equation (1), the new timescales appear in Equation (4). A typical timescale for the W variation due to the SW velocity divergence is estimated as $t_{WKB} = 2/(3|\nabla \mathbf{U}_{sw}|)$, and the timescale for wave damping by the core SW protons is $t_\gamma = 0.5/|\gamma_{sw}(k_{ext})|$. The production timescale for Alfvén wave energy is given by $t_w = (\int S_w(\mathbf{x}, k)dk/\int W(\mathbf{x}, k)dk)^{-1}$, and the typical k-space diffusion time is evaluated at $k_w = 1.5k_{min}$, giving $t_k = k_w^2/D_{kk}(\mathbf{x}, k_w)$. We did not show a typical timescale for the last term on the right-hand side of Equation (4), but $t_{WKB} < t_{LS} < t_r$. Note that t_γ characterizes the typical damping time for the wave energy around k_{ext} only. The total energy damping rate, if defined as $(2\int|\gamma_{sw}|Wdk/\int Wdk)^{-1}$, is about four orders of magnitude larger than t_γ, and it practically coincides with t_w starting from about 10 AU.

Figure 6 gives us a time hierarchy of the Alfvén energy evolution. The radial transport scales dominate all the other timescales starting from about 10 AU. The intersection of the t_w and t_{WKB} profiles at this heliocentric distance indicates that local wave generation starts to dominate the WKB attenuation. In other words, a combined effect of the WKB attenuation, large-scale driving, and the PUI generated waves in Equation (4) changes sign in the region around 10 AU, and an effective turbulence sink, not related to the wave damping by the core SW, is replaced by the energy source. Note, however, that nearly all the locally generated wave energy is damped locally by the core SW protons starting from about 10 AU, and so the total wave energy profile is simply governed by the WKB attenuation and the large-scale shear driving. Starting from about 10 AU, almost the entire dynamics of the PUI generated waves takes place locally with a superimposed slow radial transport, WKB attenuation, and the large-scale shear driving. Isotropization of the newly born PUIs takes place on a timescale less than $t_\mu = 5\times10^4$ s $\approx$ 0.6 days, ending up with the wave PSD source (8). The wave energy generated by PUIs during this timescale is much smaller compared to the total wave energy as indicated by the t_w profile. Despite t_γ being the smallest timescale in Figure 6, Alfvén waves generated around k_w cannot directly interact with the core SW protons. In this case, spectral energy transfer supplies wave energy in the k-region of damping on a timescale of $t_k \sim 10^5$–10^6 s $\approx$ 1.2–11.6 days, making

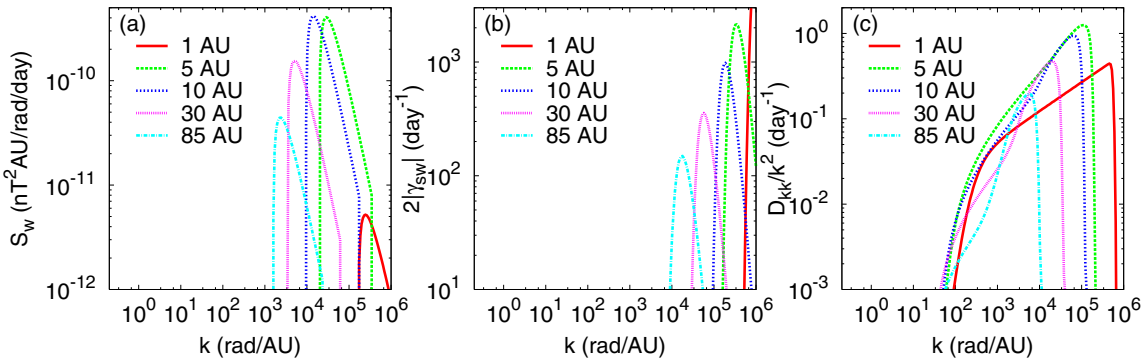

Figure 5. (a) Source of the wave PSD (8) for the different heliocentric locations along the selected SW stream line. (b) Same as (a), except for the wave damping rate (6). (c) Same as (a), except for the k-space diffusion coefficient (10).

(A color version of this figure is available in the online journal.)

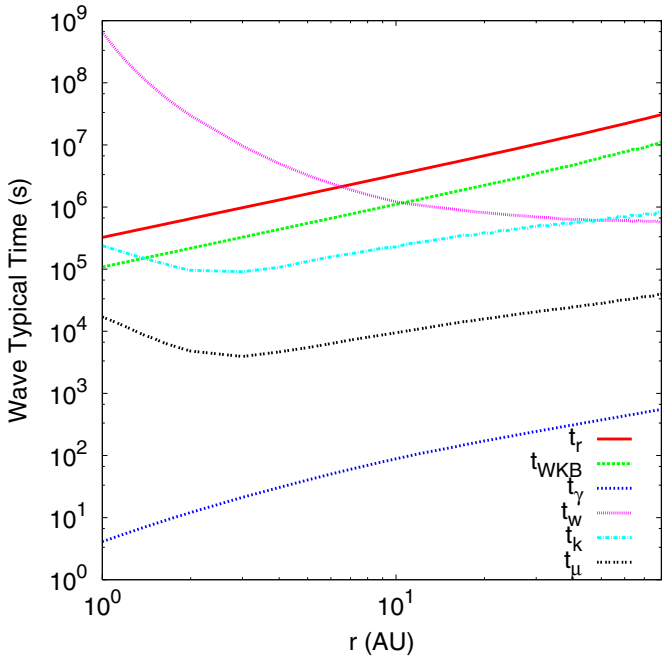

Figure 6. Radial profiles of timescales for wave fluctuations derived from Equation (4). t_{WKB} is the typical timescale for the W variation due to divergence of the SW velocity, t_γ is the timescale for wave damping by the core SW protons, t_w is the timescale for the Alfvén wave energy production, and t_k is the typical diffusion timescale in the wave number space.

(A color version of this figure is available in the online journal.)

wave dissipation possible. The transferred wave energy almost instantly damps in the dissipation region with a typical timescale of $t_\gamma \sim 10^2$–10^3 s. A superimposed large-scale radial evolution of the Alfvénic turbulence is slow and has a timescale of $t_r \sim t_{WKB} \sim t_{LS} \sim 10^7$ s ≈ 116 days.

Another important conclusion can be drawn from the comparison of the t_w and t_k profiles in Figure 6. These two profiles intersect at the heliocentric distance $\approx$45 AU, while the profiles are close enough starting from $\sim$10 AU. This means that the typical timescale for the Alfvén wave energy production is comparable to the timescale for the nonlinear wave energy cascading. This suggests that spectral features of the PUI generated waves may be observed in the wave PSD. An excitation of the low-frequency waves by the newly born PUIs in SW has been observed only sporadically, and primarily during the quasi-radial IMF conditions. The waves generated by the interstellar pickup H^+ have been observed in the *Ulysses* magnetic field data (Murphy et al. 1995). Recently, Joyce et al. (2010) have analyzed the magnetic field fluctuations measured by the MAG instrument on the *V2* spacecraft during 4.5 hr on DOY 7, 1979 at a heliocentric radial distance of 4.5 AU. They have observed spectral enhancements in the magnetic field PSD. The frequency range and polarization of the enhanced fluctuations are consistent with waves generated by the newly ionized interstellar H^+ and He^+. They have also compared the observations with a theoretical model describing wave growth due to the newly born PUIs and found a reasonable agreement between them. The event reported by Joyce et al. (2010) is the first indication of the PUI generated waves seen at *V2*, and also the first identification of the pickup He^+ waves by any spacecraft.

The Alfvén wave PSD for $C_{sh} = 1.4$, $\sigma_D = -1/3$ (the nominal case used through this study) is shown in Figure 7(a), while the PSD for $C_{sh} = 1, \sigma_D = -1/3$ is shown in Figure 7(b). The wave PSD at $r = 1$ AU is just a boundary distribution (14). Subsequent radial transport causes the wave attenuation up to the TS. In the case where there is no large-scale driving ($C_{sh} = \sigma_D = 0$), it would be a usual WKB attenuation when $W \sim r^{-3}$, but for the nominal case, the WKB attenuation is modified by the large-scale driving and $W \sim r^{-1.6}$ ($W \sim r^{-2}$ in Figure 7(b)). At the same time, concurrent wave energy injection/generation in the plasma (see Figure 5(a)), with the following k-space diffusion (see Figure 5(c)), modifies the initial shape of the wave PSD. First, because the typical timescale for the Alfvén wave energy production is comparable to the typical timescale for the nonlinear wave energy cascading, we observe in Figures 7(a) and (b) the spectral features of a newly injected wave energy starting from $\sim$10 AU. The appearance of these PUI related features in the wave PSD was predicted in previous works (e.g., Williams & Zank 1994). However, this wave enhancement cannot be reliably verified by the available observations because the reported wave enhancements are sporadic and obtained at heliocentric radial distances of only several AU (Murphy et al. 1995; Joyce et al. 2010). Second, the diffusion term in Equation (4) causes both effective PSD transport in k-space (the $\partial D_{kk}/\partial k \times \partial W/\partial k$ term) and "pure" diffusion (the $D_{kk}\partial^2 W/\partial k^2$ term). A majority of the k-transport is directed into the region of smaller k because, as follows from Figure 5(c), $\partial D_{kk}/\partial k > 0$ on the left from the D_{kk} maximum. This feature appears in Figures 7(a) and (b). The wave damping by the core SW protons controls the PSD cutoff at the large wave numbers following from the comparison of Figures 7(a) and (b) with Figure 5(b).

Figure 7(c) shows the radial profiles of the squared magnetic field for Alfvénic fluctuations, i.e., $B_w^2(\mathbf{x}) = 8\pi \int W(\mathbf{x}, k)dk$. Four model cases are shown: the WKB approximation where

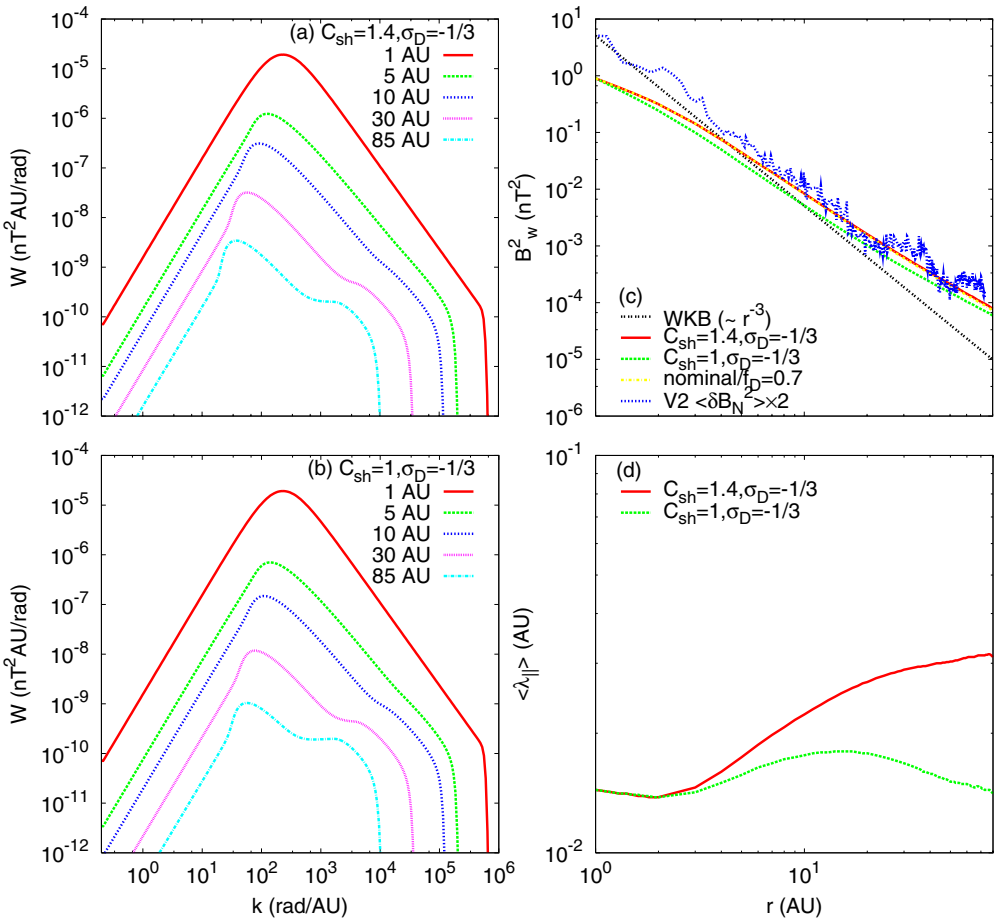

Figure 7. (a) Alfvén wave PSD for different heliocentric locations along the selected SW stream line. (b) Same as (a), except for $C_{\rm sh} = 1$, $\sigma_D = -1/3$. (c) Radial profiles of the squared magnetic field for Alfvénic fluctuations. (d) Radial profiles of the average field-aligned wavelength.

(A color version of this figure is available in the online journal.)

$B_{\rm w}^2 \sim r^{-3}$; the nominal case; the result for a smallest large-scale driving, i.e., $C_{\rm sh} = 1, \sigma_D = -1/3$; and the "nominal/$f_D = 0.7$" case where $f_D = 0.7$ is used instead of $f_D = 1$. The fifth profile in Figure 7(c) shows $2\langle \delta B_{\rm N}^2 \rangle$—the variance of the N-component of the IMF (in the standard R, T, N heliospheric coordinate system) extracted from *V2* observations (Smith et al. 2006) and then multiplied by a factor of two. The *V2* magnetic field data are obtained from the NSSDC, and the variances of the N-component are computed over 10 hr intervals. These variances are then averaged over 0.5 AU, which provides greater smoothing than the values presented in Smith et al. (2006). The N-component is half the total magnetic variance (e.g., Smith et al. 2006; Isenberg et al. 2010; Oughton et al. 2011), and so, the obtained $\langle \delta B_{\rm N}^2 \rangle$ is multiplied by a factor of two to obtain the total magnetic variance. Note that the boundary value adopted in this study for the slab component, i.e., $B_{\rm slab}^2(r = 1\,{\rm AU}) = 0.9\,{\rm nT}^2$ in Equation (14), constitutes about 18% of the total magnetic variance, $2\langle \delta B_{\rm N}^2 \rangle$, measured by *V2* at 1 AU.

The nominal $B_{\rm w}^2$ profile almost coincides with the "nominal/$f_D = 0.7$" profile, demonstrating weak dependence on f_D. The nominal profile and profile for $C_{\rm sh} = 1, \sigma_D = -1/3$, are close to each other indicating a quite weak dependence on the strength of the large-scale driving in the $C_{\rm sh}$ range obtained from the *Ulysses* data, i.e., for $C_{\rm sh} = 1$–1.5. Comparison with the *V2* data shows that the total transverse magnetic fluctuations (quasi-two-dimensional and slab components) extracted from the *V2* data agree very well with the model slab component starting from about 8 AU. This result is supported by the low-latitude observations reported by Smith (2003) and Bieber et al. (1996), which can be interpreted as indicating that the larger distances are associated with increasing energy in the slab component. For example, the slab fraction was often $\gtrsim$50% in 1992 when *Ulysses* was at about 5 AU and low latitudes. A dominance of the slab component also agrees with the model results presented by Oughton et al. (2011) where they showed that the slab component starts to dominate the two-dimensional component at heliocentric distances beyond ~10 AU. So it is likely that the slab component at low-latitudes makes up a majority of the total transverse magnetic fluctuations starting from about 8–10 AU, while this component contributes only about 20% in the total fluctuation energy at 1 AU.

The radial profiles of the average field-aligned wavelength are shown in Figure 7(d). The average wavelength is calculated as

$$\langle \lambda_{\parallel}(\mathbf{x}) \rangle = 2\pi \frac{\int k^{-1} W(\mathbf{x}, k)\, dk}{\int W(\mathbf{x}, k)\, dk},$$

and we presented two cases in Figure 7(d). In the case of smallest large-scale driving ($C_{\rm sh} = 1$, $\sigma_D = -1/3$), the $\langle \lambda_{\parallel} \rangle$ profile reflects a dominance in the wave PSD in the PUI generated short wave scales beyond ~10 AU (see Figure 7(b)). In the nominal

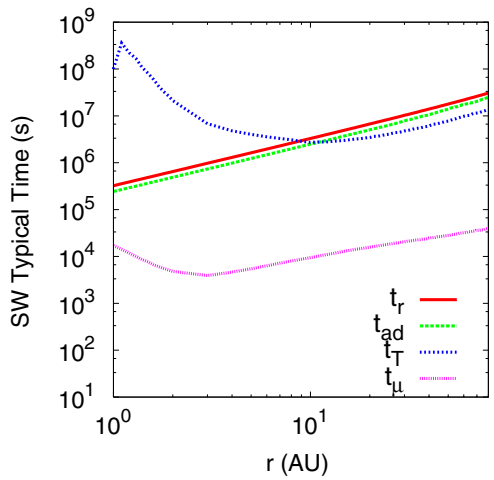

Figure 8. Radial profiles of timescales for the core SW temperature derived from Equation (12). t_{ad} is the typical timescale for adiabatic cooling of the core SW protons, and t_T is the timescale for the core SW temperature production due to the Alfvén wave energy dissipation.

(A color version of this figure is available in the online journal.)

case, the large-scale driving leads to a less rapid decrease in the wave PSD, and $\langle\lambda_\parallel\rangle$ is about two times larger at the TS.

3.3. Core SW Heating

As before, we first show in Figure 8 the typical timescales for the core SW temperature following from Equation (12). The new scales shown are the typical timescale for adiabatic cooling of the core SW protons, $t_{ad} = 3/(2|\nabla \mathbf{U}_{sw}|)$, and a timescale for the core SW temperature production due to the Alfvén wave dissipation defined as $t_T = (2S_T/(3T_{sw}n_{p,sw}k_B))^{-1}$. The timescale hierarchy in Equation (12) is similar to that in Equation (1), except that the core SW temperature production is slightly faster compared to the typical PUI production time. The t_T and t_{ad} profiles intersect at the heliocentric distance 10 AU. This indicates that the wave induced core SW heating starts to dominate adiabatic cooling beyond ~10 AU, while adiabatic cooling mostly controls the SW temperature profile in the region $r \lesssim 10$ AU. As we already mentioned, commenting on Figure 6, a combined effect of the WKB attenuation, large-scale driving, and the PUI generated waves in Equation (4) results in an effective turbulence sink in the region $r \lesssim 10$ AU, while wave energy is pumped into the turbulence beyond 10 AU. Without energy pumping, the nonlinear energy cascade to the larger wave numbers is suppressed in the region $r \lesssim 10$ AU, supplying only a small energy fraction into the region of the resonant ion cyclotron dissipation by the core SW. As a result, adiabatic cooling controls the model core SW temperature in the region $r \lesssim 10$ AU.

Figure 9(a) shows the temperature profiles for the core SW protons obtained from the *V2* observations. We used the daily average data from the MIT *Voyager 2* data site. Two temperature profiles are plotted; the original data are plotted every 10 days, and a smooth curve is constructed from the original date using the piecewise cubic polynomials whose coefficients are found by weighting the original data points. The smooth *V2* profile is similar to the 51 day running average profile of the *V2* data shown in Figure 5 of Isenberg et al. (2003). We use the smooth temperature profile to compare with the model calculations.

The smooth *V2* temperature profile, along with the model calculations for different setups, is shown in Figure 9(b). Starting from about 2 AU, the *V2* data are well above adiabatic profile ($T_{sw} \sim r^{-4/3}$), while data are well approximated by this profile inside the region 1–2 AU. The observed core SW temperature, on average, gradually decreases with distance up to about 8 AU. Then, the temperature grows over about 2 AU and reaches nearly the same value that SW had at 1 AU. In the region ~10–20 AU, the temperature sharply decreases by more than an order of magnitude, ending with the temperature slightly above adiabatic temperature at 20 AU (compare the original profile in Figure 9(a) and the adiabatic profile in Figure 9(b) at 20 AU). On average, the temperature starts to rise again for $r \gtrsim 20$ AU. The observed SW temperature profile can be broken out in at least three segments with qualitatively different radial dependencies: $r \lesssim 8$ AU, 8 AU $\lesssim r \lesssim 20$ AU, and $r \gtrsim 20$ AU. This may suggest that previous attempts to fit the temperature profile with a single power law in the region $r \lesssim 20$ AU may not have been adequate. This also suggests that the resonant wave energy dissipation may not contribute essentially to the core SW temperature in the region $r \lesssim 20$ AU. The core SW temperature

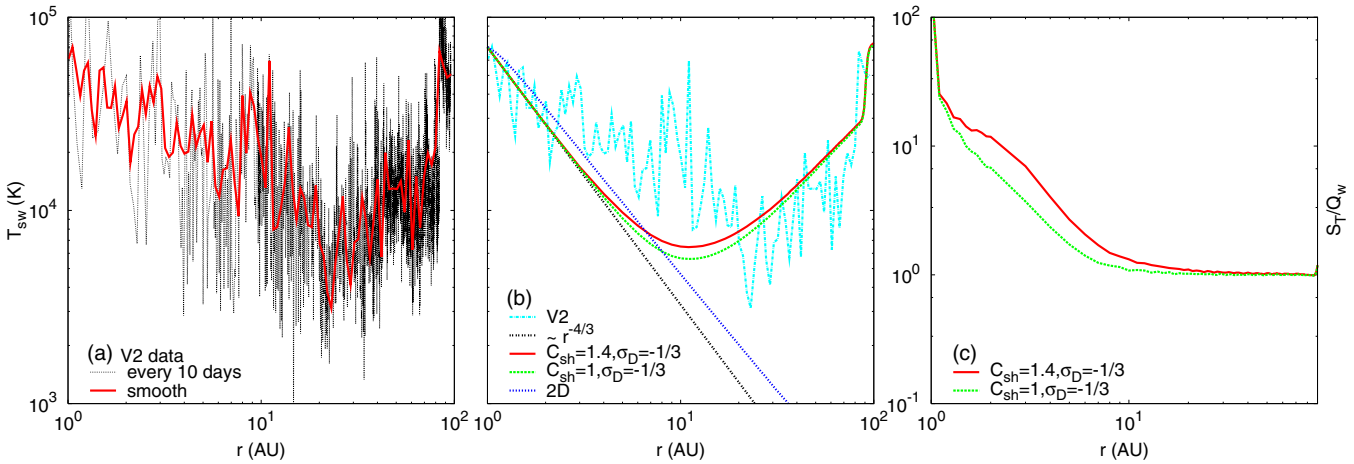

Figure 9. (a) Temperature profiles for the core SW protons along the *V2* trajectory. The daily average data are plotted every 10 days along with the daily average smooth result. (b) *V2* smooth temperature profile and the model calculations for different setups. (c) Ratio of the wave induced core SW heating rate to the wave energy production rate by the PUIs, i.e., $S_T(\mathbf{x})/Q_w(\mathbf{x})$.

(A color version of this figure is available in the online journal.)

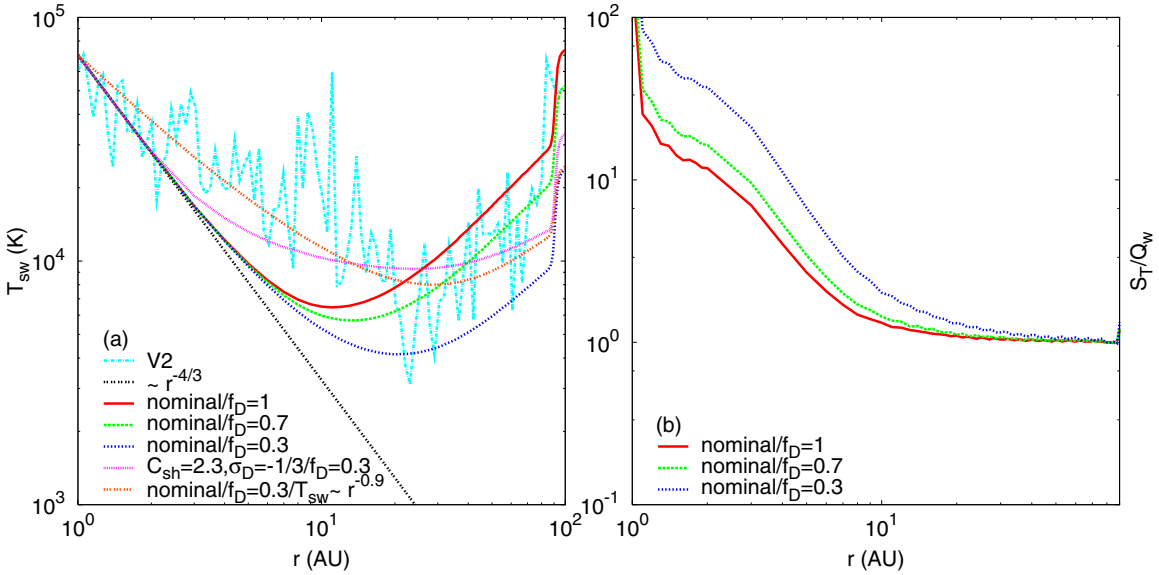

Figure 10. (a) *V2* smooth temperature profile and the model calculations for different setups. (b) Same as Figure 9(c), except the dependence on f_D is shown.
(A color version of this figure is available in the online journal.)

observed in the region $r \lesssim 20$ AU is likely to be controlled by the large-scale SW structures and their evolution. Currently, our model does not include the physics needed to account for the *V2* temperature observations in the region $r \lesssim 20$ AU because the employed version of the global MHD-plasma/kinetic-neutral model does not include the large-scale SW structures and their evolution. On the other hand, the observed SW temperature profile in the region $r \gtrsim 20$ AU, on average, may be a result of the Alfvén wave energy dissipation due to the resonant ion cyclotron interaction with the core SW protons.

In Figure 9(b), both the nominal case and the result for a smallest large-scale driving are well below the *V2* profile for 2 AU $\lesssim r \lesssim$ 20 AU, while they reproduce the observed SW temperature reasonably well for the larger heliocentric distances (recall that we use $f_D = 1$ in Figure 9(b)). So the model temperature profiles disagree with the *V2* observations in the region 2 AU $\lesssim r \lesssim$ 20 AU. Note that the SW deceleration due to the PUIs is included in our model, resulting in a higher core SW temperature in the outer heliosphere compared to the case of the constant SW speed (Isenberg et al. 2010). The "2D" profile shows the core SW temperature obtained in the case of heating by the two-dimensional turbulence, but this case will be discussed separately in Section 4.

Figure 9(c) shows the ratio of the wave induced core SW heating rate to the wave energy production rate by the PUIs, i.e., $S_T(\mathbf{x})/Q_w(\mathbf{x})$. In both cases shown, almost all the PUI generated wave energy goes into the core SW heating for $r \gtrsim 10$ AU. In the nominal case, an elevated ratio for $r \lesssim 10$ AU is due to the large-scale driving, and it is not related to the PUIs. Note that, despite the fact that S_T/Q_w is very large for the small heliocentric distances, the energy source in Equation (12) is still small compared to the adiabatic term. Because there is no pumping of the turbulent energy in this region, the nonlinear energy cascade into the dissipation region is suppressed. As a result, adiabatic cooling mostly controls the model SW temperature in the region $r \lesssim 10$ AU (see Figures 8 and 9(b)).

The model results shown in Figures 9(b) and (c) are obtained for $f_D = 1$. This value of f_D follows from the quasi-linear consideration of the PUI isotropization if there are no preexisting background waves. However, as we noted above, $f_D = 1$ should be considered as an upper limit for the wave energy injected in plasma during the PUI isotropization. For example, Williams et al. (1995, their Figure 3) adopted $f_D = 0.02$ to fit the model profile to the core SW temperature observed by *V2*. While the Williams et al. temperature profile in the region $r \gtrsim 20$ AU goes below our profiles shown in Figure 9(b), and the SW/neutral parameters used in our model differ from the parameters utilized by Williams et al., this cannot account for such a large difference in f_D. It should be noted, however, that Isenberg et al. (2003, their Figure 5) presented a SW temperature profile that is quite similar to the Williams et al. profile, but Isenberg et al. used $f_D \approx 0.31$. Thus, it is difficult to reconcile the Williams et al. and the Isenberg et al. choices for f_D, given both papers provided close SW temperature profiles. The fraction f_D used by Isenberg et al. (2003) is relatively close to the fraction used in our calculations, and the difference may be attributed to the differences in the governing equations and the SW/neutral parameters used in our model and in the Isenberg et al. model, as well as to the difference in the temperature profiles. In addition, Oughton et al. (2011) used $f_D \approx 0.5$ in their calculations, where a good agreement with the *V2* temperature was also demonstrated.

Figure 10 shows the effect of the f_D choice on the core SW temperature profile and ratio $S_T(\mathbf{x})/Q_w(\mathbf{x})$. We show the nominal case from Figures 9(b) and (c) along with the results obtained from the "nominal/$f_D = 0.7$" and the "nominal/$f_D = 0.3$" simulations. For illustration purposes only, we also show in Figure 10(a) two additional profiles: the "$C_{sh} = 2.3$, $\sigma_D = -1/3/f_D = 0.3$" profile and the "nominal/$f_D = 0.3/T_{sw} \sim r^{-0.9}$" profile, which is obtained for the "nominal/$f_D = 0.3$" setup but with a modified Equation (12) where we included an additional heating term to create an adiabatic temperature dependence as $T_{sw} \sim r^{-0.9}$. It follows from Figure 10(b) that, independent of f_D, there is some heliocentric distance beyond which the rate of the wave energy generation by PUIs is nearly balanced by the wave damping due to the resonant ion cyclotron interaction with the core SW protons, i.e., $2\int \gamma_{sw} W dk + \int S_w dk \approx 0$. We already mentioned this feature when commenting on Figure 6. The radial distance to this critical point increases with a decrease of f_D, being roughly controlled

by the location where the local wave energy generation in Equation (4) starts to dominate the energy attenuation due to a combined effect of the WKB attenuation and large-scale driving. In addition, we need to take into account a typical spatial scale for the spectral energy transfer from the k-region of wave generation into the region of wave damping by the core SW to allow an approximate balance between turbulence source and sink. The dependence of the SW temperature profile on f_D can now be easily understood (compare the "nominal/$f_D = 1$," "nominal/$f_D = 0.7$," and "nominal/$f_D = 0.3$" cases in Figure 10(a)). First, the location of temperature minimum can be estimated to be the location of the critical point identified above. Then, as follows from Equation (12), an interplay between the adiabatic cooling and the wave induced heating determines the minimum of T_{sw}. This minimum can be estimated by substituting Q_w instead of S_T in Equation (12).

It follows from the "nominal/$f_D = 1$," "nominal/$f_D = 0.7$," and "nominal/$f_D = 0.3$" results shown in Figure 10(a) that we can improve the overall agreement between the model temperature profile and the *V2* observations in the region $r \gtrsim 20$ AU by making a reasonable adjustment to f_D. The values around 0.7 give a good agreement with the *V2* profile, and they are close to the previously used values for f_D (e.g., Oughton et al. 2011). In addition, the fraction f_D should not be very small compared to unity because the Alfvénic turbulence locally generated by PUIs dominates the slab turbulence transported from the Sun at heliocentric distances beyond ~10 AU. This is also the case as follows from Figure 10(a).

The model–data agreement in the region $r \lesssim 20$ AU cannot be improved so easily and naturally as for $r \gtrsim 20$ AU. The energy source in Equation (12) is small at the heliocentric distances less than the minimum location of the core SW temperature, and adiabatic cooling controls the model temperature profile in this region. Contrary to this, the model core SW temperature profile in the region before temperature minimum has a larger than $-4/3$ spectral index in all previous works (e.g., Williams et al. 1995; Smith et al. 2001, 2006; Isenberg et al. 2003; Ng et al. 2010; Oughton et al. 2011). For example, Williams et al. (1995) added an additional heating term directly in Equation (12) to obtain the index -0.9. In principle, we can increase the strength of the large-scale driving in our model to make the temperature profile in the region $r \lesssim 20$ AU shallower than $T_{sw} \sim r^{-4/3}$. An example of such calculation is shown in Figure 10(a) as the "$C_{sh} = 2.3$, $\sigma_D = -1/3/f_D = 0.3$" profile. The increased strength of the large-scale driving shifts the boundary between an effective turbulence sink and source in Equation (4) closer to the Sun, making the nonlinear energy cascade to the larger wave numbers develop at distances closer to the Sun. As a result, more turbulent energy is supplied into the k-region of the resonant ion cyclotron dissipation by the core SW protons. Overall agreement between the "$C_{sh} = 2.3$, $\sigma_D = -1/3/f_D = 0.3$" temperature profile and the *V2* observations is reasonably good in the entire simulation region inside the TS. However, the increased shear strength is too large compared to the C_{sh} range derived by Breech et al. (2008) from the *Ulysses* data. In addition, the resulting B_w^2 profile (not shown) goes higher than the *V2* profile shown in Figure 7(c). So we do not believe that an increase in the large-scale driving is the right way to improve the agreement between the model temperature profile and the *V2* observations in the region $r \lesssim 20$ AU. The "$C_{sh} = 2.3$, $\sigma_D = -1/3/f_D = 0.3$" profile is shown in Figure 10(a) for illustration purposes only, and it should not be considered as an attempt to improve the model–*V2* agreement.

The difference between, for example, our "nominal/$f_D = 0.7$" temperature profile in the region $r \lesssim 20$ AU and the temperature profiles shown in previous works is due to the difference between the dissipation term utilized in Equation (4) and the energy decay term in the turbulence transport equations used, for example, by Smith et al. (2001, 2006), Isenberg et al. (2003), Ng et al. (2010), and Oughton et al. (2011). As a consequence, the source term on the right-hand side of Equation (12) is smaller than an adiabatic term in the region before the temperature minimum location. The small magnitude of this term has nothing to do with the particular dissipation mechanism utilized in Equation (4), but is due to the lack of wave energy transferred by the nonlinear processes into the dissipation k-region (compare temperature profiles in Figure 10(a) for the nominal and "$C_{sh} = 2.3$" cases). Indeed, there is no turbulent energy pumping in the region $r \lesssim 10$ AU (we have an effective energy sink there), and the nonlinear energy cascade into the dissipation region is suppressed. On the other hand, the source term, for example, in Equation (3) from the paper by Isenberg et al. (2003), corresponds to the case where a fully developed nonlinear cascade is comparable to the adiabatic term in the equation. In other words, only a small fraction of wave energy injected in the SW due to the large-scale driving in the region $r \lesssim 10$ AU can be transferred into the dissipation k-region and thus be dissipated by the core SW protons.

Of course, there is a possibility that an additional heating term may appear directly in Equation (12) (not through the resonant ion cyclotron interaction of the core SW with waves) to counteract adiabatic cooling, and so make the temperature profile shallower in the region $r \lesssim 20$ AU. For demonstration purposes, the calculated profile for this case is shown in Figure 10(a) as the "nominal/$f_D = 0.3/T_{sw} \sim r^{-0.9}$" profile. This profile demonstrates an improved agreement with the *V2* data in the region $r \lesssim 20$ AU, so we may assume that the compressional term $\sim(\nabla \mathbf{U}_{sw} - U_{sw,r}2/r)$ in Equation (12) may play an essential role in the region $r \lesssim 20$ AU. (Note that we do not discuss the latitudinal effects on the core SW temperature measured by *V2* because we only present the model solutions along one SW stream line.) The term $\sim(\nabla \mathbf{U}_{sw} - U_{sw,r}2/r)$ is currently negligible in Equation (12). However, it is interesting to note that, as follows from Figure 9(a), the temperature profile in the region 1 AU $\leqslant r \lesssim 20$ AU starts with an adiabatic-like behavior and ends with the temperature only slightly above the adiabatic temperature at 20 AU, while this profile is strongly non-adiabatic in between. This may indicate that compressions and rarefactions nearly compensate each other in this region. In this case, the term $\sim(\nabla \mathbf{U}_{sw} - U_{sw,r}2/r)$ may indeed operate in the region $r \lesssim 20$ AU in addition to the adiabatic cooling term ($\sim U_{sw,r}2/r$), providing almost no net heating at 20 AU compared to the adiabatic temperature. For example, it might be possible that the large-scale SW structures such as corotating interaction regions contribute to this compression term.

4. SW HEATING BY TWO-DIMENSIONAL TURBULENCE

The slab fraction of turbulence was often $\gtrsim$50% in 1992 when *Ulysses* was at about 5 AU and low latitudes, while observations at 1 AU show that this fraction constitutes only about 20% of the total fluctuation energy. This observational trend was recently demonstrated in the model calculations presented by Oughton et al. (2011). They found that the slab component starts to dominate the two-dimensional component at heliocentric distances

beyond ∼10 AU. Our own independent comparison presented in this study shows that the total transverse magnetic fluctuations (quasi-two-dimensional and slab components) extracted from the *V2* data agree well with the model slab component, with the appropriate choice of parameters, starting from about 8 AU. So it is likely that the slab component at low latitudes makes up a majority of the total transverse magnetic fluctuations starting from about 8–10 AU. However, this component contributes only about 20% to the total fluctuation energy at 1 AU. In this situation, our conclusion that dissipation of the slab component in the region $r \lesssim 10$ AU does not contribute essentially to the core SW heating does not make much sense unless the contribution of the two-dimensional component in the heating is known. So we are going to estimate the ability of the two-dimensional turbulence to heat the core SW. The idea is to model the two-dimensional component with the quasi-perpendicular to the IMF wave vector but still use damping rate (6) instead of the Landau damping for the kinetic Alfvén waves. In this setup, if we find that a nonlinear energy cascade to the larger wave numbers is suppressed in the region $r \lesssim 10$ AU, then the two-dimensional turbulence cannot contribute essentially to the core SW heating in this region. In the opposite case, when the nonlinear energy cascade is developed, we need to model the two-dimensional component with a realistic damping rate to obtain the core SW heating.

The effect of the slab component on the two-dimensional turbulence is small (Oughton et al. 2011). To model the two-dimensional component, we can use Equation (4) but with the following modifications. (1) We set $S_w = 0$ (e.g., Oughton et al. 2011), (2) the denominator in Equation (10) should be replaced by unity (e.g., Zhou & Matthaeus 1990; Jiang et al. 2009), and (3) $B^2_{slab} = 0.9$ in Equation (14) should be replaced by $B^2_{2D} \approx 0.82/0.18 \times B^2_{slab} = 4.1\,\mathrm{nT}^2$. The "2D" profile in Figure 9(b) shows the core SW temperature obtained in the case of heating by the two-dimensional turbulence. It follows from Figure 9(b) that the slope of the "2D" profile in the vicinity of 1 AU is smaller than an adiabatic slope. There is also no energy in the PSD beyond the damping rate minimum (not shown). Therefore, damping rate (6) is able to absorb all the wave energy transferred in the dissipation *k*-region. While clear evidence of the energy cascading into the dissipation region is seen in the vicinity of 1 AU, the "2D" temperature around 1 AU cannot be considered as a reliable model result because we did not use a realistic damping rate for the two-dimensional component. Actually, the *V2* data are well approximated by the adiabatic profile inside 1–2 AU, and it is unlikely that the two-dimensional component contributes to the core SW heating even in the vicinity of 1 AU. Then, the "2D" profile becomes nearly parallel to the adiabatic profile shortly after 1 AU. This means that a nonlinear energy cascade to the larger wave numbers is weak for the two-dimensional component, and adiabatic cooling mostly controls the model SW temperature in the region $r \lesssim 10$ AU. This is similar to the case of the slab component. Thus, resonant dissipation of both the slab and two-dimensional turbulent components is small in the region $r \lesssim 10$ AU, and they do not contribute essentially to the core SW heating in this region.

5. SUMMARY AND CONCLUSIONS

In this study, we have presented a self-consistent model of the interstellar pickup protons, the slab component of the Alfvénic turbulence, and the core SW protons in the outer heliosphere, $r \geqslant 1$ AU, along with the initial results and comparisons with the *V2* observations. A set of three governing equations has been used. Two kinetic equations have been used for the pickup proton PSDF and Alfvénic PSD to describe the wave–particle interaction. The proton kinetic equation includes spatial transport with the SW velocity, adiabatic cooling, diffusion in the velocity phase space, and a source of the pickup protons due to the charge exchange between the interstellar H and the core SW protons. The wave kinetic equation includes transport with the SW, the resonant wave damping by the core SW protons, the wave energy source due to isotropization of the newly born interstellar pickup protons, the driving effect of the SW flow shear and/or compression, and the wave energy diffusion in the wave number space due to the nonlinear wave–wave interaction. A fraction of the PUI free energy, which is actually released in waveform during the PUI isotropization, has been taken from the quasi-linear consideration of the PUI isotropization in the case where there are no preexisting background waves whereas we have used observations to specify the strength of the large-scale driving. Finally, to close the PUIs–waves–SW chain, we have included the core SW evolution in our model. In this initial study, we have considered the core SW protons only, omitting the other SW ions and electrons. We have further assumed that the core SW protons have a Maxwellian distribution in the frame comoving with the bulk SW flow. Then, a three-dimensional distribution of the core SW proton density has been taken from the global MHD-plasma/kinetic-neutral model of the heliosphere–LISM interaction. In this approach, the core SW temperature equation is only needed to describe SW evolution. This equation is well known, and it includes adiabatic cooling of the core SW protons along with the energy source due to the Alfvén wave dissipation.

The main results of our study can be summarized as follows.

1. For the strength of large-scale driving $C_{sh} \approx 1$–1.5 and the fraction of the bispherical wave energy $f_D \approx 0.7$–1, the model slab component agrees well with the *V2* observations of the total transverse magnetic fluctuations (quasi-two-dimensional and slab components) starting from about 8–10 AU (see Figure 7(c)). So it is likely that the slab component at low latitudes makes up a majority of the total transverse magnetic fluctuations beyond ∼8–10 AU.
2. The model core SW temperature profile agrees well with the *V2* observations in the region $r \gtrsim 20$ AU if a fraction $f_D \approx 0.7$–1 of the bispherical wave energy is injected into the background Alfvénic turbulence during PUI isotropization (see Figure 10(a)).
3. The combined effect of the WKB attenuation, large-scale driving, and the PUI generated waves in Equation (4) results in an effective energy sink in the region $r \lesssim 10$ AU, while wave energy is pumped into the turbulence beyond 10 AU. Without energy pumping, the nonlinear energy cascade to the larger wave numbers is suppressed in the region $r \lesssim 10$ AU, supplying only a small energy fraction into the region of the resonant ion cyclotron dissipation by the core SW protons. A similar situation takes place for the two-dimensional turbulent component, where the nonlinear energy cascade is also weak.
4. The energy source due to the resonant Alfvén wave damping by the core SW protons is small at heliocentric distances $r \lesssim 10$ AU for both the slab and two-dimensional turbulent components. As a result, an adiabatic cooling mostly controls the model SW temperature in the region $r \lesssim 10$ AU, and the model temperature profile disagrees with the *V2* observations in the region $r \lesssim 20$ AU.

We thank Charles Smith for providing fluctuations of the *N*-component of the magnetic field and the MIT Space Plasma Group for making the *Voyager* data available online at http://web.mit.edu/space/www/voyager/voyager.html. This work was supported in part by DOE grant DE-SC0008334, NASA grants NNX09AG29G, NNX09AB24G, NNX09AG63G, NNX12AB30G, and by the NSF grants AGS-1156056, and AGS-1203516.

REFERENCES

Akhiezer, A. I., Akhiezer, I. A., Polovin, R. V., Sitenko, A. G., & Stepanov, K. N. 1975, Plasma Electrodynamics, Vol. 1 (Tarrytown, NY: Pergamon)
Barnett, C. F. 1990, Atomic Data for Fusion, Vol. 1, Collisions of H, H_2, He and Li Atoms and Ions with Atoms and Molecules, Tech. Rep. ORNL–6086/VI (Oak Ridge, TN: Oak Ridge Nat. Lab.)
Bieber, J. W., Matthaeus, W. H., Smith, C. W., et al. 1994, ApJ, 420, 294
Bieber, J. W., Wanner, W., & Matthaeus, W. H. 1996, J. Geophys. Res., 101, 2511
Breech, B., Matthaeus, W. H., Minnie, J., et al. 2005, Geophys. Res. Lett., 32, L06103
Breech, B., Matthaeus, W. H., Minnie, J., et al. 2008, J. Geophys. Res., 113, A08105
Burlaga, L. F., Ness, N. F., Belcher, J. W., et al. 1994, J. Geophys. Res., 99, 21511
Chalov, S. V., Alexashov, D. B., & Fahr, H.-J. 2006, Astron. Lett., 32, 206
Dasso, S., Milano, L. J., Matthaeus, W. H., & Smith, C. W. 2005, ApJ, 635, L181
Fahr, H. J. 1971, A&A, 14, 263
Fahr, H. J., & Chashei, I. V. 2002, A&A, 395, 991
Florinski, V., Zank, G. P., Heerikhuisen, J., Hu, Q., & Khazanov, I. 2010, ApJ, 719, 1097
Florinski, V., Zank, G. P., & Pogorelov, N. V. 2003, J. Geophys. Res., 108, 1228
Galeev, A. A., & Sagdeev, R. Z. 1988, Astrophys. Space Sci., 144, 427
Gary, S. P., & Madland, C. D. 1988, J. Geophys. Res., 93, 235
Heerikhuisen, J., Pogorelov, N. V., Florinski, V., Zank, G. P., & le Roux, J. A. 2008, ApJ, 682, 679
Hollweg, J. V. 1974, J. Geophys. Res., 79, 1539
Huddleston, D. E., & Jonstone, A. D. 1992, J. Geophys. Res., 97, 12217
Isenberg, P. A. 1986, J. Geophys. Res., 91, 9965
Isenberg, P. A. 1997, Geophys. Res. Lett., 24, 623
Isenberg, P. A. 2005, ApJ, 623, 502
Isenberg, P. A., Smith, C. W., & Matthaeus, W. H. 2003, ApJ, 592, 564
Isenberg, P. A., Smith, C. W., Matthaeus, W. H., & Richardson, J. D. 2010, ApJ, 719, 716
Jiang, Y., Liu, S., & Petrosian, V. 2009, ApJ, 698, 163
Joyce, C. J., Smith, C. W., Isenberg, P. A., Murphy, N., & Schwadron, N. A. 2010, ApJ, 724, 1256
Kennel, C. F., & Petschek, H. E. 1966, J. Geophys. Res., 71, 1
Kucharek, H., & Scholer, M. 1995, J. Geophys. Res., 100, 1745
le Roux, J. A., & Webb, G. M. 2009, ApJ, 693, 534
Matthaeus, W. H., Oughton, S., Pontius, D. H., & Zhou, Y. 1994, J. Geophys. Res., 99, 19267
Matthaeus, W. H., Zank, G. P., & Oughton, S. 1996, J. Plasma Phys., 56, 659
McComas, D. J., Alexashov, D., Bzowski, M., et al. 2012, Science, 336, 1291
Milano, L. J., Dasso, S., Matthaeus, W. H., & Smith, C. W. 2004, Phys. Rev. Lett., 93, 155005
Murphy, N., Smith, E. J., Tsurutani, B. T., Balogh, A., & Southwood, D. J. 1995, Space Sci. Rev., 72, 447
Ng, C. S., Bhattacharjee, A., Munsi, D., Isenberg, P. A., & Smith, C. W. 2010, J. Geophys. Res., 115, A02101
Oughton, S., Matthaeus, W. H., Smith, C. W., Breech, B., & Isenberg, P. A. 2011, J. Geophys. Res., 116, A08105
Pogorelov, N. V., Heerikhuisen, J., & Zank, G. P. 2008, ApJ, 675, L41
Pogorelov, N. V., Stone, E. C., Florinski, V., & Zank, G. P. 2007, ApJ, 668, 611
Roberts, D. A., Goldstein, M. L., Klein, L. W., & Matthaeus, W. H. 1987a, J. Geophys. Res., 92, 12023
Roberts, D. A., Klein, L. W., Goldstein, M. L., & Matthaeus, W. H. 1987b, J. Geophys. Res., 92, 11021
Ruciński, D., Cummings, A. C., Gloeckler, G., et al. 1996, Space Sci. Rev., 78, 73
Schlickeiser, R. 1989, ApJ, 336, 243
Smith, C. W. 2003, in AIP Conf. Proc. 679, Solar Wind Ten, ed. M. Velli, R. Bruno, & F. Malara (Melville, NY: AIP), 413
Smith, C. W., Isenberg, P. A., Matthaeus, W. H., & Richardson, J. D. 2006, ApJ, 638, 508
Smith, C. W., Matthaeus, W. H., Zank, G. P., et al. 2001, J. Geophys. Res., 106, 8253
Stone, E. C., Cummings, A. C., McDonald, F. B., et al. 2005, Science, 309, 2017
Toptygin, I. N. 1985, Cosmic Rays in Interplanetary Magnetic Fields (Dordrecht: Reidel)
Williams, L. L., & Zank, G. P. 1994, J. Geophys. Res., 99, 19229
Williams, L. L., Zank, G. P., & Matthaeus, W. H. 1995, J. Geophys. Res., 100, 17059
Wu, C. S., & Davidson, R. C. 1972, J. Geophys. Res., 77, 5399
Zank, G. P., Dosch, A., Hunana, P., et al. 2012, ApJ, 745, 35
Zank, G. P., Matthaeus, W. H., Bieber, J. W., & Moraal, H. 1998, J. Geophys. Res., 103, 2085
Zank, G. P., Matthaeus, W. H., & Smith, C. W. 1996, J. Geophys. Res., 101, 17093
Zhou, Y., & Matthaeus, W. H. 1990, J. Geophys. Res., 95, 14881